Evaporation of sulphate aerosols at low relative humidity

Georgios Tsagkogeorgas[1], Pontus Roldin[2,3], Jonathan Duplissy[2,4], Linda Rondo[5], Jasmin Tröstl[6], Jay G. Slowik[6], Sebastian Ehrhart[5a], Alessandro Franchin[2], Andreas Kürten[5], Antonio Amorim[7], Federico Bianchi[2], Jasper Kirkby[5,8], Tuukka Petäjä[2], Urs Baltensperger[6], Michael Boy[2], Joachim Curtius[5], Richard C. Flagan[9], Markku Kulmala[2,4], Neil M. Donahue[10], Frank Stratmann[1]

[1]Leibniz Institute for Tropospheric Research, 04318, Leipzig, Germany
[2]Department of Physics, University of Helsinki, P.O. Box 64, 00014, Helsinki, Finland
[3]Division of Nuclear Physics, Lund University, P.O. Box 118, 221 00, Lund, Sweden
[4]Helsinki Institute of Physics, University of Helsinki, P.O. Box 64, 00014 Helsinki, Finland
[5]Institute for Atmospheric and Environmental Sciences, Goethe University Frankfurt, 60438, Frankfurt am Main, Germany
[6]Paul Scherrer Institute, CH–5232, Villigen, Switzerland
[7]Fac. Ciencias & CENTRA, Universidade de Lisboa, Campo Grande, 1749–016, Lisboa, Portugal
[8]CERN, CH–1211, Geneva, Switzerland
[9]California Institute of Technology, Pasadena, CA 91125, USA
[10]Center for Atmospheric Particle Studies, Carnegie Mellon University, Pittsburgh, PA 15213, USA
[a]now at: Atmospheric Chemistry Department, Max Planck Institute for Chemistry, 55128, Mainz, Germany

Correspondence to: Georgios Tsagkogeorgas (george.tsagkogeorgas@tropos.de)

Abstract. Evaporation of sulphuric acid from particles can be important in the atmospheres of Earth and Venus. However, the equilibrium constant for the dissociation of H_2SO_4 to bisulphate ions, which is the one of the fundamental parameters controlling the evaporation of sulphur particles, is not well constrained. In this study we explore the volatility of sulphate particles at very low relative humidity. We measured the evaporation of sulphur particles versus temperature and relative humidity in the CLOUD chamber at CERN. We modelled the observed sulphur particle shrinkage with the ADCHAM model. Based on our model results, we conclude that the sulphur particle shrinkage is mainly governed by H_2SO_4 and potentially to some extent by SO_3 evaporation. We found that the equilibrium constants for the dissociation of H_2SO_4 to HSO_4^- ($K_{H_2SO_4}$) and the dehydration of H_2SO_4 to SO_3 ($^xK_{SO_3}$) are $K_{H_2SO_4}=2$–$4\cdot10^9$ mol·kg^{-1} and $^xK_{SO_3}\geq1.4\cdot10^{10}$ at 288.8±5 K.

Key words: sulphate aerosol evaporation, sulphuric acid dissociation, sulphuric acid equilibrium constants, sulphuric acid vapour pressure, water activity, activity coefficients, Earth's and Venus' stratospheres, ADCHAM, CLOUD experiment

1 Introduction

Suspended particulate matter in the atmosphere plays a key role in Earth's climate. Atmospheric aerosol particles affect the amount of solar radiation absorbed by the Earth system. This is accomplished either when atmospheric aerosol particles directly absorb or scatter incoming solar energy (causing warming or cooling), or when particles act as cloud condensation or ice nuclei

(leading to an increase in cloud albedo, which causes cooling). A substantial fraction of particle number and mass across a wide range of environmental conditions arises from sulphur emissions (Clarke et al., 1998a; Turco et al., 1982).

Sulphur in Earth's atmosphere in turn originates from natural phenomena like volcanic eruptions and biota decomposition. Violent volcanic eruptions can loft sulphur dioxide (SO_2) to the stratosphere, which can then form sulphur aerosol particles. Those sulphur aerosols can remain suspended in the stratosphere for ~1–2y before falling into the troposphere (Wilson et al., 1993; Deshler, 2008). The three main natural agents for sulphate aerosol formation in troposphere are dimethyl sulphide (DMS), which arises from marine phytoplankton decomposition (Charlson et al., 1987; Kiene, 1999; Simó and Pedrós–Alió, 1999), SO_2, which occurs naturally as a decay product of plant and animal matter (Grädel and Crutzen, 1994; Hübert, 1999; Capaldo et al., 1999), and carbonyl sulphide (OCS), which is emitted from anaerobic biological activity and provides the main non–volcanic flux of sulphur into the stratosphere (Galloway and Rodhe, 1991; Rhode, 1999).

The atmospheric sulphate burden is substantially perturbed by sulphur emissions associated with anthropogenic activities. The largest anthropogenic source of sulphur is fossil–fuel combustion; coal is the predominant source, but also heavy fuel oil is important (Öm et al., 1996; Smith et al., 2001). Fossil–fuel combustion constitutes ~⅔ of the total global sulphur flux to the atmosphere (Rhode, 1999; Wen and Carignan, 2007), and dominates emissions in most populated regions. Other anthropogenic factors also affect the sulphuric acid (H_2SO_4) budget, notably sulphur aerosol formation in aircraft plumes (Fahey et al., 1995; Curtius et al., 1998), and extensive sulphur use in industry with a direct environmental impact on local scale. However, on a regional to global scale the acidification of fresh water and forest ecosystems is mainly caused by wet and dry deposition of SO_2 and sulphate particles (Simpson et al., 2006).

Sulphur is also a crucial constituent in Venus' atmosphere, an environment with very low relative humidity (RH) (Moroz et al., 1979; Hoffman et al., 1980a), forming the main cloud layer in the form of sulphuric acid droplets (Donahue et al., 1982), which are maintained in an intricate photochemical cycle (photooxidation of OCS, Prinn 1973). Sulphuric acid's reaction paths remain a subject of investigation (Zhang et al., 2010), which makes the study of the sulphur cycle (including the sulphur species SO, SO_2, SO_3, H_2SO_4) an important endeavour for understanding both the chemistry and climate of Venus (Mills et al., 2007; Hashimoto and Abe, 2000).

H_2SO_4 serves as an effective nucleating species and, thus, strongly influences atmospheric new–particle formation (Laaksonen and Kulmala, 1991; Weber et al., 1999; Kulmala et al., 2000; Yu and Turco, 2001; Fiedler et al., 2005; Kuang et al., 2008). The nucleation rate, which is the formation rate ($cm^{-3} \cdot s^{-1}$) of new particles at the critical size, strongly depends upon the saturation ratio of H_2SO_4. Uncertainty in this ratio results in an uncertainty of several orders of magnitude in the calculated nucleation rate (Roedel, 1979). To model the excess H_2SO_4 responsible for the gas–to–particle conversion it is necessary to know the vapour pressure of H_2SO_4 over sulphuric acid and/or neutralized solutions.

The sulphuric acid vapour pressure appears through the free–energy term in the exponent of the new–particle formation rate (Volmer and Weber, 1926; Stauffer, 1976). Quantitative theoretical predictions of nucleation rates are highly uncertain because the pure H_2SO_4 equilibrium vapour pressure is not well known (Gmitro and Vermeulen, 1964; Doyle, 1961;

Kiang and Stauffer, 1973). However, accurate calculations of the H_2SO_4 vapour pressure require accurate equilibrium rate constant values to constrain the reactions of formation and dissociation of H_2SO_4 in aqueous solutions.

While H_2SO_4 is often presumed to be practically non–volatile, this is not always the case. There are several circumstances on Earth and Venus where the vapour pressure of H_2SO_4 matters; specifically, at very low RH, high temperature (T), when there is a deficit of stabilizing bases, and when particles are very small. A very important region of Earth's environment is the upper stratosphere where these conditions prevail (Vaida et al. 2003). Under these conditions H_2SO_4 can evaporate from particles. This can either inhibit growth of nanoparticles or lead them to shrink.

Furthermore, molecular H_2SO_4 is never the dominant constituent in sulphuric acid solutions. It will completely dehydrate to sulphur trioxide (SO_3, which is extremely volatile) in a truly dry system and yet almost entirely dissociate into bisulphate ion (HSO_4^-) and hydronium cation (H_3O^+) in the presence of even trace water (H_2O) (Clegg and Brimblecombe, 1995). This is why H_2SO_4 is such a powerful desiccant. Also, bases such as ammonia (NH_3) will enhance chemical stabilization and form sulphate salts. The thermodynamics of the H_2SO_4–H_2O system at low RH are uncertain, so we seek to improve our understanding of this part of the phase diagram. To accomplish this, we measured the shrinkage of nearly pure H_2SO_4 particles in the CLOUD chamber at CERN at very low RH and then simulated these experiments with an aerosol dynamics model coupled with a thermodynamics model to constrain the equilibrium constants, for the dissociation $K_{H_2SO_4}$ and the dehydration ${}^x K_{SO_3}$, of H_2SO_4 coupling HSO_4^-, H_2SO_4, and SO_3. These new values can be used in models that simulate the evolution of sulphate aerosol particles in the atmospheres of Venus and Earth.

2 Aqueous phase sulphuric acid reactions

H_2SO_4 dissociation and potential dehydration to SO_3 are the principal subjects of this study. In aqueous solutions H_2SO_4 can dissociate in two steps.

$$H_2SO_{4(aq)} \xleftrightarrow{\quad K_{H_2SO_4} \quad} HSO_{4(aq)}^- + H^+ \tag{R1}$$

$$HSO_{4(aq)}^- \xleftrightarrow{\quad K_{HSO_4^-} \quad} SO_{4(aq)}^{2-} + H^+ \tag{R2}$$

H_2SO_4 partially dissociates to form HSO_4^- via reaction 1 (R1). $K_{H_2SO_4}$ represents the equilibrium constant for R1. HSO_4^- can then undergo a second dissociation reaction (R2) to form a sulphate ion (SO_4^{2-}). In above reactions, sulphur's oxidation number is 6 (S(VI)).

For dilute aqueous solutions, R1 is considered to be complete. However, when the mole fraction of S(VI) exceeds ~0.5, H_2SO_4 can be detected in the solution (Walrafen et al., 2000; Margarella et al., 2013). When H_2SO_4 is present in the solution, dehydration of H_2SO_4 to form SO_3 (R3) can also be important (Wang et al., 2006; Que et al., 2011). ${}^x K_{SO_3}$ represents the equilibrium constant for R3 on a mole fraction basis.

$$SO_{3(aq)} + H_2O \xleftrightarrow{\quad {}^x K_{SO_3} \quad} H_2SO_{4(aq)} \tag{R3}$$

3

NH₃, which mainly originates from anthropogenic agriculture emissions, is the most abundant base in atmospheric secondary aerosol particles. NH₃ neutralises sulphuric acid particles by reacting with H^+ and forming an ammonium ion (NH_4^+) (R4).

$$NH_{3(aq)} + H^+ \xleftrightarrow{\quad K_{NH_3} \quad} NH_4^+ \tag{R4}$$

Even in the cleanest environments, such as the stratosphere, NH₃ is present at low concentrations and $NH_{3(g)}$ will be dissolved in the acidic sulphate particles.

3 Methods

In the CLOUD (Cosmics Leaving OUtdoor Droplets, Kirkby et al. (2011)) chamber at CERN, we measured the H₂SO₄ aerosol evaporation process under precisely controlled temperature and relative humidity. We designed experiments to accomplish a gradual decrease of RH (from 11.0 to 0.3 %) under atmospherically relevant conditions. To understand the processes governing the measured particle evaporation, we modelled the experiments with the Aerosol Dynamics, gas– and particle–phase chemistry model for laboratory CHAMber studies (ADCHAM, Roldin et al., 2014).

3.1 Experimental set up

Details of the CLOUD chamber, the main element of the experimental set up can be found in Kirkby et al. (2011) and Duplissy et al. (2016). For the experiments described here, we formed and grew sulphuric acid particles in the chamber by oxidising SO₂ with OH radicals that were generated by photolysing O₃ and allowing the resulting O(^{1}D) to react with water vapour. During these experiments we fed the aerosol population to an array of instruments for characterisation of both physical and chemical properties.

We utilized the following instruments to measure gas-phase concentrations: a SO₂ monitor (Enhanced Trace Level SO₂ 15 Analyser, Model 43i–TLE, Thermo Scientific, USA), an O₃ monitor (TEI 49C, Thermo Environmental Instruments, USA) and a Chemical Ionisation Mass Spectrometer (CIMS) measured the gas–phase H₂SO₄ concentration ([H₂SO₄$_{(g)}$] between ~$5 \cdot 10^5$ and ~$3 \cdot 10^9$ cm^{-3}, Kürten et al., 2011; Kürten et al., 2012). The CIMS data provided the total gaseous sulphuric acid concentration, [H₂SO₄$_{(g)}$] without constraining the hydration state of the evaporating molecules (e.g. H₂SO₄ associated with one, two, or three H₂O molecules).

We measured the evolution of the aerosol number size distribution with a Scanning Mobility Particle Sizer (SMPS, Wang and Flagan, 1990), which recorded the dry particle mobility diameter in the size range from about 10 to 220 nm. We operated the SMPS system with a recirculating dried sheath flow (RH<14 % controlled by a silicon dryer) with a sheath to aerosol sample flow ratio of 3:0.3 L. We maintained the Differential Mobility Analyser (DMA) and recirculating system at 278–288 K by means of a temperature control rack, while we operated the Condensation Particle Counter (CPC) at room

temperature. We corrected the SMPS measurements for charging probability, including the possibility of multiple charges, diffusion losses, and CPC detection efficiency.

We measured aerosol particle chemical composition with an Aerodyne Aerosol Mass Spectrometer (AMS) quantifying sulphate, nitrate, ammonium and organics for particles between 50 and 1000 nm aerodynamic diameter (Jimenez et al., 2003a; Drewnick et al., 2006; Canagaratna et al., 2007). The AMS provided the mass concentration measurements ($\mu g \cdot m^{-3}$) calculated from the ion signals by using measured air sample flow rate, nitrate ionization efficiency (IE) and relative IE of the other species.

3.2 The experimental procedure

To study aerosol particle evaporation, the formation of sulphuric acid particles preceded. At the lowest H_2O levels (*RH<11 %*) and in the presence of O_3, controlled UV photo–excitation reactions initiated the oxidation of SO_2 to H_2SO_4. Sulphuric acid particles nucleated and grew to a size of ~220 nm by condensation of $H_2SO_{4(g)}$ at a quasi–constant gas phase concentration (~$1\cdot10^9$ cm^{-3} with an uncertainty of >20 %). The H_2SO_4 formation and particle growth ended when we closed the shutters in the front of the UV light source. Afterwards, we induced particle shrinkage by decreasing the RH. We decreased the RH in two separate ways; either by minimizing the influx of water vapour to the chamber, or by increasing the temperature. This separation in experimental procedures gave the ability to achieve and control extremely low RH values (Table 1).

After the end of the particle formation period and during the initial steps of evaporation, before the RH started to decrease, the aerosol size distribution remained nearly constant. Subsequently, the RH decreased gradually initiating the particle evaporation. When the RH reached a certain low value (*RH≤1.5 % for T=288.8* K) the particles shrank rapidly, as revealed by the SMPS measurements, and the [$H_2SO_{4(g)}$] increased until it reached a peak value (see Supplement, Fig. S1). The [H_2SO_4]$_{peak}$ was significantly higher than the background concentration before the onset of evaporation (Table 1). After reaching a maximum in gas–phase concentration, the sulphuric acid decreased again, though the size distribution remained stable (e.g., ~50 (±10) nm for experiments 1 and 2, see Sect. 4.3) depending on the RH and T conditions. This behaviour revealed that the remaining aerosol could not be pure sulphuric acid, but rather consisted of a more stable chemical mixture that inhibited further evaporation.

Similarly, the AMS recorded the evaporation of particles (see Supplement, Fig. S1). The AMS measurements showed that the particles were composed almost exclusively of sulphuric acid (but not pure H_2SO_4). Based on AMS data, calculations of the kappa value (κ), which is defined as a parameter that describes the aerosols water uptake and cloud condensation nucleus activity (CCN activity), (Petters and Kreidenweis, 2007) of the mixed particles as a function of time during particle evaporation (see Supplement, Fig. S2) yield a value close to the κ for pure sulphuric acid particles (Sullivan et al., 2010). A κ value is indicative of the solubility of aerosol particles, with *κ=0* referring to an insoluble particle and *κ=0.7* to pure sulphuric acid particles. κ is computed by the approximate equation, Eq. (1)

$$\kappa = \frac{4 \cdot A^3}{27 \cdot D_d^3 \cdot ln^2 S_c} \tag{1}$$

when the critical diameter D_d and critical saturation S_c (or supersaturation, s_c, when referring to CCN activity) are known. The term A can be calculated from the water properties.

3.3 The model framework

In the present work we use ADCHAM (Roldin et al., 2014, 2015) to study the evolution of the particle number size distribution and particle chemical composition. Instead of simulating the new–particle formation in the CLOUD chamber, we use the measured particle number size distribution before the UV–lights are turned off as well as time sequences of RH, T and [$H_2SO_{4(g)}$] as inputs to the model (Fig. 1). In order to capture the evolution of the particle number size distribution we consider Brownian coagulation, particle wall deposition, condensation and evaporation of H_2SO_4, SO_3 and H_2O from the particles.

3.3.1 The activity coefficients

Within an aqueous electrolyte solution, such as the H_2SO_4–SO_3–H_2O system, cations, anions and molecular species all disrupt ideality. Here, we consider interactions between ions (HSO_4^-, SO_4^{2-}, NH_4^+, H^+) and molecules (H_2SO_4, SO_3, H_2O) in the particle–phase chemistry model. To calculate the molality based activity coefficients for the inorganic ions (γ_i) and the mole fraction based activity coefficient for water (f_{H_2O}) we apply the Aerosol Inorganic Organic Mixtures Functional groups Activity Coefficients (AIOMFAC) model (validated at room temperatures, Zuend et al., 2008 and 2011). The reference state for ions and water in the model is an infinitely dilute aqueous solution ($\gamma_i(\chi_{H_2O} \to 1)=1$ and $f_{H_2O}(\chi_{H_2O} \to 1)=1$.

For relatively dilute $H_2SO_{4(aq)}$ solutions (low solute concentration), typical for most atmospheric conditions, it is reasonable to assume that the dissociation of H_2SO_4 to HSO_4^- (R1) is complete (Clegg et al., 1998, Zuend et al., 2008). However, in this work we demonstrate that this assumption fails at low RH and also for small particles with a large Kelvin term. Furthermore, at a very low water activity (a_w) (less than ~0.01) a non–negligible fraction of the H_2SO_4 could potentially decompose to SO_3 (R3); if this is the case, the thermodynamic model need to consider not only R1 but R3 as well (Fig. 1).

Since AIOMFAC does not consider inorganic non–electrolyte compounds like H_2SO_4 and SO_3 we implement additionally to this the symmetric electrolyte–NonRandom Two–Liquid (eNRTL) activity coefficient model (Bollas et al., 2008, Song and Chen, 2009) which is optimized for the H_2SO_4–H_2O–SO_3 systems by Que et al., (2011). In this work we use the regressed eNRTL binary interaction parameters from Que et al., 2011. Following the convention of the eNRTL model (Chen et al., 1982), we set the unknown binary parameters for NH_4^+–molecule, molecule–NH_4^+ and NH_4^+–ions to – 4, 8 and 0, respectively.

The reference state of the molecular species in eNRTL is defined as the pure liquid. eNRTL provides mole fraction based activity coefficients for H_2SO_4 and SO_3, $f_{H_2SO_4}$ and f_{SO_3}, respectively. ADCHAM calculates $f_{H_2SO_4}$ and f_{SO_3} as a function of a_w and N:S, $\chi_{N(-III)}$:$\chi_{S(VI)}$ (Fig. S3). The modelled $f_{H_2SO_4}$ and f_{SO_3} approach unity not only at the standard state of the pure liquids ($f_{H_2SO_4}(\chi_{H_2SO_4} \to 1)=1$ and $f_{SO_3}(\chi_{SO_3} \to 1)=1$), but also for the infinitely dilute aqueous solution ($f_{H_2SO_4}(\chi_{H_2O} \to 1)=1$ and $f_{SO_3}(\chi_{H_2O} \to 1)=1$). This is because the eNRTL binary H_2O–H_2SO_4 and H_2O–SO_3 interaction parameters are zero

in the model. For all conditions between these limiting states, the short–range ion (HSO_4^-, SO_4^{2-}, NH_4^+, H^+) –molecule (H_2SO_4, SO_3) interactions, and Pitzer–Debye–Hückel long–range ion–molecule interactions influence the modelled $f_{H_2SO_4}$ and f_{SO_3}. At $T=288.8$ K, $f_{H_2SO_4}$ reaches the highest values (~2.29) when $a_w \approx 0.25$ and f_{SO_3} reaches the highest values (~1.95) when $a_w \approx 0.35$ (Fig. S3). We also assume that the activity coefficient of NH_3 is unity for the model simulations. However, sensitivity tests performed for $\gamma_{NH_3}=0.1$ and $\gamma_{NH_3}=10$ reveal that, for the acidic particles ($N:S<1$), our model results are completely insensitive of the absolute value of γ_{NH_3}.

3.3.2 The particle phase composition

If ammonium cation (NH_4^+) is present in the sulphuric acid particles, then solid ammonium bisulfate ($NH_4HSO_4(s)$) may form when the S(VI) and H_2O start to evaporate from the particles. However, the particles may also stay as highly supersaturated droplets with respect to the crystalline phase (Zuend et al., 2011). The particle number size distribution measurements in our experiments did not indicate a sudden drop in particle size during evaporation, which would be expected if the particles crystalized and all particle water was suddenly removed. Thus, in the present work we do not consider formation of any solid salts. We further neglect the influence of any mass–transfer limitations in the particle phase, and assume that the particle ion–molecule equilibrium composition (R1–R3) and water content can be modelled as equilibrium processes (because they are established rapidly compared to the composition change induced by the evaporation of H_2SO_4 and SO_3). We use the thermodynamic model to update the particle equilibrium water content, mole fractions and activity coefficients of all species. Then the model considers the gas–particle partitioning of H_2SO_4 and SO_3 with a condensation algorithm in the aerosol dynamics model (Sect. 3.3.5). The time step set in the model is 1s.

The thermodynamic model uses an iterative approach to calculate the particle equilibrium mole fractions of H_2O, H_2SO_4, SO_3, HSO_4^-, SO_4^{2-}, NH_3, NH_4^+ and H^+, based on the current time step, known RH, and absolute number of moles of S(VI) and N(–III) for each particle size bin. The modelled particle–phase mole fraction of N(–III) during the evaporation experiments is always substantially lower than that of S(VI) ($N:S<0.7$). For these particles the saturation vapour pressure of NH_3 is always less than 10^{-10} Pa, within the experimental water activity range 0–0.11 and $\gamma_{NH_3} \geq 0.1$. Thus, it is reasonable to assume that during the experiments NH_3 does not evaporate from the particles.

Based on the particle diameters from the previous time step (which depend on the particle water content), the thermodynamic model starts by calculating a_w for each particle size, considering the Kelvin effect. Given a_w, the model estimates the particle water mole fraction. Then the model calculates the H^+ molality in the aqueous phase via a 4th order polynomial, derived from the ion balance equation, Eq. (2) in combination with the thermodynamic equilibrium constant equations, Eq. (3–6), and the S(VI) and N(–III) mole balance equations, Eq. (7–8). The maximum positive real root of this polynomial gives the H^+ concentration, [H^+].

$$\left[H^+ \right] + \left[NH_4^+ \right] = \left[HSO_4^- \right] + 2 \left[SO_4^{2-} \right] \tag{2}$$

$$K_{H_2SO_4} = \frac{[HSO_4^-] \cdot \gamma_{HSO_4^-} \cdot [H^+] \cdot \gamma_{H^+}}{[H_2SO_4] \cdot \gamma_{H_2SO_4}} \tag{3}$$

$$K_{HSO_4^-} = \frac{[SO_4^{2-}] \cdot \gamma_{SO_4^{2-}} \cdot [H^+] \cdot \gamma_{H^+}}{[HSO_4^-] \cdot \gamma_{HSO_4^-}} \tag{4}$$

$$^xK_{SO_3} = \frac{\chi_{H_2SO_4} \cdot f_{H_2SO_4}}{\chi_{SO_3} \cdot f_{SO_3} \cdot \chi_{H_2O} \cdot f_{H_2O}} \tag{5}$$

$$K_{NH_3} = \frac{[NH_3] \cdot \gamma_{NH_3} \cdot [H^+] \cdot \gamma_{H^+}}{[NH_4^+] \cdot \gamma_{NH_4^+}} \tag{6}$$

5   $$n_{S(VI)} = n_{H_2SO_4} + n_{HSO_4^-} + n_{SO_4^{2-}} + n_{SO_3} \tag{7}$$

$$n_{N(-III)} = n_{NH_4^+} + n_{NH_3} \tag{8}$$

The thermodynamic equilibrium coefficients for H_2SO_4 and HSO_4^- dissociations and NH_3 protonation (Eq. 3, 4 and 6) are given in a molality based form while the equilibrium coefficient in Eq. (5), which involves the equilibration between the different solvents (H_2O, SO_3 and H_2SO_4), is given in a mole fraction based form. The Eq. (5) is given in a mole fraction based

10   form for the following reasons: a) the eNRTL provides mole fraction based activity coefficients, and b) if Eq. (5) would be applied for a_w that are even lower than considered in this work, the assumption of using molalities, i.e. where water is considered to be the only solvent, will not be acceptable. The model calculates $K_{HSO_4^-}$ and K_{NH_3} (mol·kg^{-1}) with Eq. (9) and Eq. (10) (Jacobson, 2005a). We treat $K_{H_2SO_4}$ and $^xK_{SO_3}$ as unknown model fitting parameters.

$$K_{HSO_4^-} = 1.015 \cdot 10^{-2} \cdot e^{\left(8.85 \cdot \left(\frac{298}{T} - 1\right) + 25.14 \cdot \left(1 + \ln\left(\frac{298}{T}\right) - \frac{298}{T}\right)\right)} \tag{9}$$

15   $$K_{NH_3} = 1.7882 \cdot 10^9 \cdot e^{21.02 \cdot \left(\frac{298}{T} - 1\right)} \tag{10}$$

Once [H$^+$] is determined, all other ion and molecule concentrations can be derived from Eq. (2–8). Based on the new estimated particle–phase ion and molecule mole fractions, the thermodynamic model uses AIOMFAC and eNRTL to update the ion and molecule activity coefficients. The model then repeats the whole procedure iteratively until the relative change in the concentration and activity coefficients for each compound is less than 10^{-9} between successive iteration steps. To stabilize

20   convergence, the model estimates activity coefficients used in the proceeding iteration as a weighted average of the values from the previous and present iteration time steps.

3.3.3 H_2SO_4 and SO_3 in the gas–phase

In the gas phase only a fraction of H_2SO_4 is in the form of pure sulphuric acid molecules while the rest of the H_2SO_4 is in a hydrated form. In this work we use the parameterization from Hanson and Eisele (2000), who measured the diffusion loss rate of H_2SO_4 to flow–tube walls at different RH, to estimate the RH–dependent effective diffusion coefficient of $H_2SO_{4(g)}$.

In the gas phase, SO_3 reacts rapidly with H_2O to form H_2SO_4. Based on the measured loss rate of SO_3, which shows a second–order dependence on the water vapour concentration (Jayne et al., 1997), we estimate that $SO_3(g)$ is converted to $H_2SO_{4(g)}$ in less than 1s during the CLOUD chamber experiments, even at the lowest RH. Because of this rapid conversion to H_2SO_4 and the high vapour pressure of SO_3 (Eq. 12), it is reasonable to assume that the gas–phase concentration of SO_3 (vapour pressure, $p_{\infty,SO_3(g)}$) is negligibly low.

3.3.4 Saturation vapour pressures, surface tension and particle density

We use Eq. (11) and (12) to calculate the temperature dependent sub–cooled pure–liquid saturation vapour pressures for H_2SO_4 and SO_3 ($p_{0,i}$, where i refers to H_2SO_4 or SO_3 in Pa). Equation (11) is based on the work of Ayers et al. (1980), with corrections for lower temperatures by Kulmala and Laaksonen (1990). We use the (best fit) L parameter value of $–11.695$ (Noppel et al., 2002, Noppel–Kulmala–Laaksonen, N–K–L parameterisation, see Supplement Fig. S5 (a)). Equation (12) is based on the work of Nickless (1968) (see Supplement Fig. S5 (b)).

$$p_{0,H_2SO_4} = 101325 \cdot e^{\left(L+10156\cdot\left[\frac{1}{360.15} - \frac{1}{T} + \frac{0.38}{545}\cdot\left(1+\ln\left(\frac{360.15}{T}\right) - \frac{360.15}{T}\right)\right]\right)} \tag{11}$$

$$p_{0,SO_3} = e^{\left(28.9239 - \frac{7000}{T}\right)} \cdot 133.3224 \tag{12}$$

As an alternative to Eq. (11) and (12) we also use the H_2SO_4 and SO_3 pure–liquid saturation vapour pressure parameterisations from Que et al., 2011 (originally from the Aspen Plus Databank, Fig. S5).

We calculate the saturation vapour pressures of H_2SO_4 and SO_3 for each particle size with Eq. (13), using the mole fractions ($\chi_{i,j}$) and mole fraction based activity coefficients ($f_{i,j}$) of H_2SO_4 and SO_3 (from the thermodynamic model) and the Kelvin term, $C_{k,i,j}$ Eq. (14) for compound i in particle size bin j.

$$p_{s,i,j} = p_{0,i} \cdot a_{i,j} \cdot C_{k,i,j} \tag{13}$$

where $a_{i,j} = \chi_{i,j} \cdot f_{i,j}$

$$C_{k,i,j} = e^{\left(\frac{4 \cdot M_i \cdot \sigma_j}{R \cdot T \cdot \rho_{p,j} \cdot D_{p,j}}\right)} \tag{14}$$

$a_{i,j}$ is the activity of compound i in size bin j, T is the temperature in Kelvin, R is the universal gas constant (J·mol^{-1}·K^{-1}), M_i is the molar mass (kg·mol^{-1}) of compound i, $\rho_{p,j}$ is the density (kg·m^{-3}) of the liquid particles, σ_j is the surface tension (N·m^{-1}) and $D_{p,j}$ is the particle diameter (m) of the particles in size bin j.

As an alternative approach we also model the evaporation of H_2SO_4 using composition dependent H_2SO_4 activities $(\alpha_{H_2SO_4,j})$ derived directly from the tabulated values of the difference in chemical potentials between the sulphuric acid in aqueous solution and that of the pure acid $(\mu_{H_2SO_4,j} - \mu^0_{H_2SO_4})$. The tabulated values that are valid at 298.15 K are taken from Giauque et al. (1960). The relationship between $\mu_{H_2SO_4,j} - \mu^0_{H_2SO_4}$ and $\alpha_{H_2SO_4,j}$ is given by Eq. (15).

$$\ln(a_{H_2SO_4,j}) = (\mu_{H_2SO_4,j} - \mu^0_{H_2SO_4})/(R \cdot T) \tag{15}$$

In accordance with Ayers et al. (1980) we neglect any temperature dependence of $\mu_{H_2SO_4,j} - \mu^0_{H_2SO_4}$. This empirically based approach is used in several chemistry transport models to simulate the evaporation of pure sulphuric acid particle in the stratosphere (see e.g. Kokkola et al., 2009; English et. al., 2011 and Hommel et. al., 2011).

We calculate the surface tension and density of the particles comprising a ternary mixture of water, sulphuric acid and ammonium with parameterisations given by Hyvärinen et al. (2005) that combine surface tension parameterisations for $(NH_4)_2SO_4$–H_2O mixtures (Hämeri et al., 2000, Korhonen et al., 1998b), H_2SO_4–H_2O mixtures (Vehkamäki et al., 2002) and NH_3–H_2O mixtures (King et al. 1930). For the range of conditions in our experiment, where the minimum particle diameter after evaporation is ~50(±10) nm (for experiments 1 and 2). The Kelvin effect only increases the water saturation vapour pressure by maximum value of 1.07 (and the H_2SO_4 saturation vapour pressure by 1.44, see Supplement Fig. S6) for the particle diameter of 40 nm.

3.3.5 Evaporation of H_2SO_4, SO_3 and H_2O

We model the gas–particle partitioning (evaporation) of H_2SO_4 and SO_3 using the full moving size distribution method in combination with the Analytic Prediction of Condensation, APC scheme (Jacobson, 2005a). APC is an unconditionally stable numerical discretisation scheme used to solve the condensation equation, Eq. (16). In Eq. (16), we substitute the saturation vapour pressures from Eq. (13) and the measured concentration, $C_{\infty,H_2SO_4(g)}$, (vapour pressure, $p_{\infty,H_2SO_4(g)}$) of $H_2SO_{4(g)}$. Based on the motivation given in Sect. 3.3.3 the vapour pressure of SO_3, $p_{\infty,SO_3(g)}$, is set to zero.

$$\frac{dm_{i,j}}{dt} = \frac{2 \cdot \pi \cdot (d_i + d_j) \cdot (D_i + D_j) \cdot M_i}{R \cdot T} \cdot \beta_{i,j}(Kn_{i,j}, \alpha_i) \cdot (p_{\infty,i} - p_{s,i,j}) \tag{16}$$

$$\beta_{i,j}(Kn_{i,j}, \alpha_i) = \frac{Kn_{i,j} + 1}{0.377 \cdot Kn_{i,j} + 1 + \frac{4}{3 \cdot \alpha_i} \cdot (Kn^2_{i,j} + Kn_{i,j})}$$

$$Kn_{i,j} = \frac{2 \cdot \lambda_{i,j}}{d_i + d_j}, \qquad \lambda_{i,j} = \frac{3 \cdot (D_i + D_j)}{\sqrt{v_i^2 + v_j^2}} \tag{17}$$

Equation (16) describes the contribution of species i to the mass growth rate of a particle in size bin j, $\beta_{i,j}$ is the Fuchs–Sutugin correction factor in the transition region (Fuchs and Sutugin, 1971), d_i, d_j correspond to diameters (m) and D_i, D_j to diffusion coefficients ($m^2 \cdot s^{-1}$) of the condensing molecule i and the particles in size bin j, respectively. α_i is the mass–accommodation coefficient of compounds i and $Kn_{i,j}$ is the non–dimensional Knudsen number, Eq.(17). $\lambda_{i,j}$ is the mean free path (m) and v_i, v_j are the thermal speed ($m \cdot s^{-1}$) of the molecule i and the particles in size bin j, respectively. Equations (16) and (17) take into account that the condensing molecules have a non–negligible size compared to the size of the smallest particles, and that small particles have non–negligible diffusion coefficients (Lehtinen and Kulmala, 2003).

Based on measurements of H_2SO_4 losses in a flow tube reactor, Pöschl et al., (1998) derived a mass accommodation coefficient of $H_2SO_{4(g)}$ on aqueous sulphuric acid, a_{m,H_2SO_4}, which was close to unity, with a best fit value of 0.65, a lower limit value of 0.43 and an upper limit of 1.38 (physical limit 1.0). The measured mass accommodation coefficients did not show any dependence on the relative amount of water in the particles (Pöschl et al., 1998). For the model simulations in this work we use unity mass accommodation coefficients. The particle water content is modelled as an equilibrium process with the thermodynamic model (see Sect. 3.3.2).

3.3.6 Particle losses

The electric field strength of the stainless–steel CLOUD chamber, in contrast to smog chambers made of Teflon, is very low. Therefore we can neglect electrostatic deposition enhancements (for details on how ADCHAM treats particle wall deposition losses see Roldin et al., 2014). We simulate the particle size–dependent deposition losses with the model from Lai and Nazaroff (2000). The particle deposition loss depends on the friction velocity (u^*), which we treat as an unknown model fitting parameter. The best possible agreement between the modelled and measured particle number and volume concentration in the chamber is achieved with a friction velocity of ~0.2 $m \cdot s^{-1}$. Thus, for all model results we present in this article we use $u^*=0.2$ $m \cdot s^{-1}$. Dilution losses due to the purified air injected to the CLOUD chamber are also considered in the model.

3.3.7 Constraining the thermodynamic properties of sulphate aerosol particles

We use ADCHAM to constrain the values of the thermodynamic equilibrium coefficients, $K_{H_2SO_4}$ and $^xK_{SO_3}$, by treating these coefficients as unknown model fitting parameters. By varying the equilibrium coefficients we search for the best possible agreement (coefficient of determination (R^2), see Supplement, Table S1) between the modelled and measured geometric mean diameter (GMD) with respect to particle number. Because experimental results reveal that the sulphate particles did not evaporate completely, they must have been contaminated with a small fraction of effectively non–volatile material (Sect. 3.2). In the model we address this by assuming that the particles (prior to evaporation) contained either a small fraction of

non–volatile organic material (e.g., secondary organic aerosol, SOA) or that the particles contained small amounts of ammonium, which prevented pure H_2SO_4 particle formation and consequently prevented the evaporation. We calculate the initial SOA and ammonium dry particle volume fraction in particle size bin j ($\chi^v_{SOA,j}$ and $\chi^v_{NH4^+,j}$) with Eq. (18) and (19), respectively. Here d_{SOA} and d_{NH4^+} represent an effective particle diameter of SOA and ammonium if all other particle species are removed. For experiment 1 we use $d_{SOA}=60$ nm and $d_{NH4^+}=26$ nm, for experiment 2 $d_{SOA}=43$ nm and $d_{NH4^+}=19$ nm and for experiment 3 $d_{SOA}=38$ nm and $d_{NH4^+}=17$ nm.

$$\chi^v_{SOA,j} = \min\left(\frac{d^3_{SOA}}{d^3_j}, 0.2\right) \tag{18}$$

$$\chi^v_{NH_4^+,j} = \min\left(\frac{d^3_{NH_4^+}}{d^3_j}, 0.05\right) \tag{19}$$

4 Results and discussion

In order to fit the modelled particle number size distribution evolution to the observations we performed several hundred simulations where we varied $K_{H_2SO_4}$ and $^xK_{SO_3}$. We summarize these simulations into three main categories (Cases):

1) only H_2SO_4 and H_2O evaporation ($^xK_{SO_3}=\infty$), (Case 1)

2) combination of H_2SO_4, H_2O and SO_3 evaporation, (Case 2) and

3) practically only SO_3 and H_2O evaporation, (Case 3).

Case 2 is further divided into two subcategories, Case 2a and 2b. In Case 2a the H_2SO_4 is the dominant evaporating S(VI) species while in Case 2b the SO_3 is the dominant evaporating S(VI) species.

4.1 Particle–phase mole fractions

Figure 2 shows an example of the modelled mole fractions of (**a**) $H_2SO_{4(aq)}$, $\chi_{H_2SO_4}$, and (**b**) $SO_{3(aq)}$, χ_{SO_3}, as a function of the a_w and $N:S$ for Case 2a with equilibrium constants $K_{H_2SO_4}=2.40 \cdot 10^9$ mol·kg^{-1}, and $^xK_{SO_3}=1.43 \cdot 10^{10}$ at $T=288.8$ K. Fig. 2 reveals that the increase of χ_{SO_3} as a_w decreases is steeper than for $\chi_{H_2SO_4}$. This is because $H_2SO_{4(aq)}$ formation precedes SO_3 formation (see R3). As expected, the highest values of $\chi_{H_2SO_4}$ and χ_{SO_3} occur when $N:S=0$ and a_w approaches zero. While $N:S$ increases, $\chi_{H_2SO_4}$ and χ_{SO_3} decrease gradually and reach lower values when $N:S$ become larger than 0.6.

4.2 Particle number size distribution evolution

In Figure 3 we present the particle number size distribution evolution after the shutter of the UV light is closed and the influx of water vapour to the chamber is interrupted for experiment 2, performed at $T=288.8$ K, showing (a) the measured and (b)

12

the modelled values for Case 2a with $K_{H_2SO_4}=2.40 \cdot 10^9$ mol·kg^{-1} and $^xK_{SO_3}=1.43 \cdot 10^{10}$. At the beginning of the evaporation process the particles in the size range from ~60 to ~180 nm in diameter contain approximately 70 mole % H_2O; however, this percentage decreases, declining to 15 mole % after 6 h (Fig. 3 (c)). Before H_2SO_4 and SO_3 start to evaporate from the particles the assumed mole fraction of ammonium is very low (Fig. 3 (d)). However, during the evaporation process $N:S$ increases

5   steadily until it reaches a value of ~0.6 after ~6 h. At this point the particles are ~40 nm in diameter and do not shrink further. This model result is in good agreement with the experimental results reported by Marti et al. (1997) and confirms that NH_4^+ effectively stabilizes sulphur particles against evaporation when *N:S≈0.6*. Thus, in the stratosphere, even small amounts of a base (such as NH_3) can prevent the sulphate particles from shrinking.

4.3 Geometric mean diameter shrinkage influenced by relative humidity

10   Figure 4 compares the measured and modelled GMD evolution as a function of (a) time and (b) RH for experiments 1 and 2 performed at a temperature of *T=288.8* K (Table 1) with NH_3 as a particle phase contaminant (see Supplement, Table S1, simulations 1–4 and 13–16). The pure liquid saturation vapour pressures of H_2SO_4 and SO_3 are calculated with Eq. (11) and (12). The model results are in good agreement with the measured GMD trend for Case 1 ($K_{H_2SO_4}=2.00 \cdot 10^9$ mol·kg^{-1}), Case 2a ($K_{H_2SO_4}=2.40 \cdot 10^9$ mol·kg^{-1} and $^xK_{SO_3}=1.43 \cdot 10^{10}$), Case 2b ($K_{H_2SO_4}=4.00 \cdot 10^9$ mol·kg^{-1} and $^xK_{SO_3}=1.54 \cdot 10^9$) and Case 3

15   ($K_{H_2SO_4}=1.00 \cdot 10^{11}$ mol·kg^{-1} and $^xK_{SO_3}=3.33 \cdot 10^7$). The Case 3 simulations give a particle shrinkage that begins somewhat too late and occurs somewhat too rapidly. However, considering the measurement uncertainties it is impossible to constrain the relative contribution of H_2SO_4 and SO_3 to the observed GMD loss only based on these two experiments (see Sect. 4.4).

With the Aspen Plus Databank pure liquid saturation vapour pressure parameterisations it is also possible to find similarly good agreement between the modelled and observed GMD evolution during experiment 1 and 2 for Cases 1, 2a, 2b

20   and 3 (Fig. S8) with NH_3 as the particle phase contaminant, but with somewhat different values of $K_{H_2SO_4}$ and $^xK_{SO_3}$ (see Supplement, Table S1, simulations 8–11 and 20– 23).

The model simulations with non–volatile and non–water–soluble organics or dimethylamine (DMA) as the particle phase contaminant give nearly identical results as with NH_3, both for experiments 1 and 2 (see Supplement Table S1, simulations 6, 7, 17 and 18). In the case of DMA this occurs because it is also a strong enough base to be completely protonated

25   (all N(–III) is in the form of NH_4^+). In the case of an organic contaminant instead of NH_3 the model results mainly differ at a later stage of the particle evaporation phase when the $N:S$ approaches ~0.5. This is because the evaporation rate does not slow down before all S(VI) is lost when the particles do not contain any base (see Fig. S9). Thus, the modelled GMD shrinkage becomes somewhat faster, when assume organic contamination. Without any particle phase contamination (pure sulphuric acid particles) the particles evaporate faster and completely (see Supplement, Fig. S10).

30   Instead of explicitly calculating the H_2SO_4 activity with the thermodynamic model we derive it directly from the tabulated values of the H_2SO_4 chemical potentials as a function of the molality, following Giauque et al. (1960), Eq. (15). With this method we simulate the evaporation of H_2SO_4 without explicitly calculating the concentration of H_2SO_4 in the particles.

13

However, since the tabulated chemical potentials from Giauque et al. (1960) are only valid for pure sulphuric acid solutions and temperatures close to 298.15 K it cannot be used if the particle aqueous phase also contains ammonium or other stabilizing molecules.

Based on data from Giauque et al. (1960), Eq. (15) and the pure–liquid saturation vapour pressure parameterization from N–K–L parameterisation (Noppel et al, 2002; Kulmala and Laaksonen, 1990), Eq. (11) the modelled GMD shrinkage is consistent with the observations for experiments 1 and 2, when we consider the Case 1 (H_2SO_4 as the only evaporating S(VI) species) and particle phase contamination due to non–volatile non–water–soluble organics (see Supplement, Figure S11 and Table S1, simulations 5, 12, 19 and 24). However, when we use the pure–liquid saturation vapour pressure parameterisation from the Aspen Plus Databank, the modelled particles evaporate earlier (at higher RH) than the observed particles. The reason is that the ASPEN compared to N–K–L parameterisation gives higher saturation vapour pressures (see Supplement, Fig. S5).

4.4 Geometric mean diameter shrinkage influenced by relative humidity and temperature

In an attempt to constrain how $K_{H_2SO_4}$ and $^xK_{SO_3}$ depend on the temperature, and the role of H_2SO_4 and SO_3 on the observed particle diameter shrinkage, as a next step we simulate experiment 3, which expands in temperature. For this experiment the temperature increases gradually from 268 K to 293 K while the absolute humidity remains at a constant value, thus allowing the RH to decrease. Equation (20) describes the modelled temperature dependence of $K_{H_2SO_4}$ and $^xK_{SO_3}$ where the K_i values at $T=288.8$ K ($K_{i,\ 288.8\ K}$) set equal to the values in regard to the model simulations of experiment 1 and 2 (Sect. 4.2):

$$K_i = K_{i,288.8K} \cdot e^{\left(B_i\left(\frac{1}{T} - \frac{1}{288.8}\right)\right)} \tag{20}$$

where i can be either H_2SO_4 or SO_3. With $B_i=0$ K there is no temperature dependence of K_i.

For other acids like HNO_3, HCl and HSO_4^-, K_i decreases with increasing T ($B_i>0$) (Jacobson, 2005a). Que et al. (2011) estimates $B_{H_2SO_4}$ to be 3475 K and B_{SO_3} to be 14245.7 K. Thus, based on this information we would expect the equilibrium reactions R1 and R3 to shift towards the left (more $H_2SO_{4(aq)}$ and SO_3 as temperature increases). This would result in a stronger temperature dependence of the $H_2SO_{4(aq)}$ and SO_3 saturation vapour pressures over aqueous sulphuric acid droplets (Eq. 13) compared to the temperature dependence expected if we only consider the temperature effect of the pure–liquid saturation vapour pressures (Fig. S5).

Figure 5 compares the measured and modelled GMD evolution during experiment 3. For the simulations we use either the same temperature dependence as suggested by Que et al. (2011) ($B_{H_2SO_4}=3475$ K and $B_{SO_3}=14245.7$ K), or no temperature dependence of $K_{H_2SO_4}$ and $^xK_{SO_3}$ ($B_{H_2SO_4}=0$ K and $B_{SO_3}=0$ K) or weak temperature dependence $B_{H_2SO_4}=0$ K and $B_{SO_3}=-3000$ K. One of these model simulations correspond to Case 1 and the rest to Case 2a (see Supplement, Table S1, simulation 28 and 29, 33, 34 and 36, respectively).

For the Case 1 simulation (see Supplement, Table S1, simulation 28) we use Eq. (15) and the tabulated H_2SO_4 chemical potentials from Giauque et al. (1960) to derive the H_2SO_4 activity. The particle phase contaminant is assumed to be

14

non–volatile and non–water–soluble organics. In this simulation the modelled particles grow somewhat too much before they start to shrink. For the Case 2a simulation where the temperature dependences of $K_{H_2SO_4}$ and $^xK_{SO_3}$ are described by the $B_{H_2SO_4}$ and B_{SO_3} values derived by Que *et al.* (2011) (see Supplement, Table S1, simulation 29) the model cannot capture the observed GMD evolution. For the Case 2a simulations with $B_{H_2SO_4}=0$ K and $B_{SO_3}=0$ K (see Supplement, Table S1, simulations 33 and 34) the particle phase contaminant is assumed to be NH$_3$ or non–volatile and non–water–soluble organics. These model simulations, which agree with the observed GMD, indicate that the temperature dependences of $K_{H_2SO_4}$ and $^xK_{SO_3}$ need to be very weak or insignificant ($B_{H_2SO_4}=0$ K and $B_{SO_3}=0$ K). If the particles are contaminated with NH$_3$, B_{SO_3} or $B_{H_2SO_4}$ even needs to be negative for optimum fitting (e.g. $B_{H_2SO_4}=0$ K and $B_{SO_3}=-3000$ K, see Supplement, Table S1, simulations 36). It is also possible to find good agreement between the modelled and measured GMD evolution if one of $B_{H_2SO_4}$ and B_{SO_3} is negative and the other one is positive ($B_{H_2SO_4}=3475$ K and $B_{SO_3}=-10000$ K, see Supplement, Table S1, simulation 31). The H$_2$SO$_4$ and SO$_3$ pure liquid saturation vapour pressures in these simulations are calculated with Eq. (11) and (12).

If we instead use the pure–liquid saturation vapour pressure parameterizations from the Aspen Plus Databank (which have somewhat weaker temperature dependences than Eq. 11 and 12), the model results captures the observed GMD evolution if both $B_{H_2SO_4}$ and B_{SO_3} are zero and H$_2$SO$_4$ is the only evaporating (SVI) species (Case 1, see Supplement, Table S1, simulation 50) or the main evaporating S(VI) species (Case 2a, see Supplement, Table S1, simulation 51, see Supplement, Fig. S12).

For Case 2b and 3 simulations in which we assume that SO$_3$ is responsible for most of the S(VI) evaporation, the model can never capture the observed GMD evolution. This is the case regardless of the pure liquid saturation vapour pressure method we use (N–K–L–Nickless or Aspen Plus Databank, see Supplement, Table S1, simulations 42, 48, 52 and 53) .

Based on the simulations of experiment 3 we conclude that most of the S(VI) that evaporated from the particles probably was in the form of H$_2$SO$_4$ (Cases 1 and 2a). The very weak temperature dependences for $K_{H_2SO_4}$ and $^xK_{SO_3}$ needed for the model to capture the GMD evolution during experiment 3 is surprising and calls for further investigation. Part of the explanation to this could be that the AIOMFAC activity coefficient model is developed based on experimental data derived at 298.15 K. The uncertainty arising from the two different pure liquid saturation vapour pressure parameterisations (temperature dependent) also limits our ability to fully constrain the $K_{H_2SO_4}$ and $^xK_{SO_3}$ values. Based on our experiments and model simulations the equilibrium constant $K_{H_2SO_4}$ should be somewhere in the range 2.0–4.0·10^9 mol·kg^{-1} and the $^xK_{SO_3}$ needs to be larger than 1.4·10^{10} at a temperature of 288.8 ± 5 K. The type of contamination of the sulphate particles (NH$_3$, DMA or a non–volatile non–water–soluble organic compound) does not have a substantial impact on our results and conclusions.

4.5 Atmospheric implications

In the following section, we define an effective saturation concentration of H$_2$SO$_{4(g)}$ $\left(C^*_{H_2SO_4,S}\right)$ as the sum of the saturation concentration of H$_2$SO$_4$ $\left(C_{H_2SO_4,S}\right)$ and SO$_3$ $\left(C_{SO_3,S}\right)$, based on the assumption of rapid conversion of SO$_{3(g)}$ to

15

$H_2SO_{4(g)}$, Eq. (21), (see Supplement S5, Fig. S7).

$$C^*_{H_2SO_4,S} = C_{H_2SO_4,S} + C_{SO_3,S} \tag{21}$$

Figure 6 shows the modelled effective H_2SO_4 saturation concentration $\left(C^*_{H_2SO_4,S}\right)$ as a function of particle size ($d_p = 1–10^3$ nm) and RH ($0–100\ \%$). The results are from a model simulation with $K_{H_2SO_4} = 2.40 \cdot 10^9$ mol·kg^{-1} and $^xK_{SO_3} = 1.43 \cdot 10^{10}$, $T = 288.8$ K and pure liquid saturation vapour pressures calculated with Eq. (11) and (12). The four different panels (a–d) correspond to simulations using four different values for $N:S$, namely 0, 0.5, 0.75 and 1. In each panel, the contours show the $log_{10}\left(C^*_{H_2SO_4,S}\right)$ levels. For example, the $log_{10}\left(C^*_{H_2SO_4,S}\right) = 7$ contour corresponds to an effective H_2SO_4 saturation concentration of 10^7 molecules cm^{-3}. These contours provide the H_2SO_4 gas–phase concentration at which the net flux of S(VI) to and from the particles is zero (particles neither grow nor shrink).

The observed atmospheric daytime range of the $[H_2SO_{4(g)}]$ is approximately $10^5–10^8$ molecules cm^{-3}, and so we shade this range in Figure 6. When $C^*_{H_2SO_4,S}$ is less than this range (to the upper right in the panel), the particles for most atmospheric daytime conditions will grow by condensation of H_2SO_4; when $C^*_{H_2SO_4,S}$ is greater than this (to the lower left in the panel) the particles will for most conditions shrink by evaporation of S(VI); in the shaded range the particles will tend to equilibrate. The larger the mole fraction of bases (NH_3) in the aerosol particles the less prone they will be to shrink. When particles are composed only of S(VI) and H_2O ($N:S=0$) and the concentration of $H_2SO_{4(g)}$ is 10^7 molecules cm^{-3} all particles smaller than 10 nm will shrink at $RH<13.2\ \%$. For the same $[H_2SO_{4(g)}]$ and $N:S=0.5$ all particles smaller than 10 nm shrink at $RH<12.1\ \%$. However, for $N:S=0.75$ particles smaller than 4 nm shrink at $RH<5.5\ \%$, and if $N:S=1$ only particles smaller than ~1.9 nm shrink, independent of RH except when it is extremely dry ($RH \leq 1.5\ \%$). With the vapour pressure parameterisations from the Aspen Plus Databank and $K_{H_2SO_4} = 4.00 \cdot 10^9$ and $^xK_{SO_3} = 4.55 \cdot 10^{10}$ the results are almost identical.

These model results demonstrate that sulphuric acid can evaporate from particles or be unable to contribute to their growth for atmospherically relevant conditions, characterized by low relative humility, relatively high temperatures and weak sources of NH_3 and SO_2. Such environments can be found in the stratosphere and possibly also in the troposphere over large desert regions.

5 Summary and conclusions

This study demonstrates, both experimentally and theoretically, the importance of H_2SO_4 evaporation from aerosol particles at atmospheric relevant conditions. We measured the sulphate aerosol particle shrinkage below a certain low relative humidity (e.x. $RH \lesssim 1.5\%$ for $T=288.8$ K and $RH \lesssim 0.7\%$ for $T=268.0$ K) in the CLOUD chamber at CERN. We modelled the sulphur evaporation with ADCHAM. Our model simulation show that:

    i.   the dissociation of $H_2SO_{4(aq)}$ is not complete, and evaporation of H_2SO_4 and H_2O can explain the observed particle shrinkage. However, we cannot dismiss the possibility that some of the shrinkage is due to evaporating SO_3, which is formed when $H_2SO_{4(aq)}$ is dehydrated.

16

ii.   the equilibrium rate coefficient for the first dissociation stage of $H_2SO_{4(aq)}$ ($K_{H_2SO_4}$) falls somewhere in the range *2.0– 4.0·10^9* mol·kg^{-1} at 288.8 ± 5 K.

iii.   the equilibrium coefficient for the dehydration of H_2SO_4 ($^xK_{SO_3}$) must at least be larger than 1.4·10^{10}.

The main factors limiting our estimation of $K_{H_2SO_4}$ are uncertainties in the pure liquid saturation vapour pressure of H_2SO_4
5   and the relative contribution of SO_3 to the observed particle evaporation. Other potential sources of error are the uncertainties in the derived activity coefficients, the mass accommodation coefficient of H_2SO_4 and solid salt formation during the particle evaporation phase. The model simulations of an experiment where the temperature was gradually increased from 268 to 293 K, indicates that the temperature dependencies of $K_{H_2SO_4}$ and $^xK_{SO_3}$ need to be weak. Future studies should focus on constraining the pure liquid saturation vapour pressures of H_2SO_4 and SO_3 and the temperature dependence of $K_{H_2SO_4}$ and
10    $^xK_{SO_3}$.

In order to be able to make an accurate prediction of the sulphate particles influence on global climate, their thermodynamic properties need to be properly described in global climate models. Thus, our constraints on the dissociation, $K_{H_2SO_4}$ and dehydration, $^xK_{SO_3}$ of H_2SO_4 are important contributions to the global aerosol-climate model community. The outcome of this study implies that atmospheric modelling studies, especially those dedicated to new particle formation, should
15   not by default assume that sulphate particles are non-volatile. Models that exclude the evaporation process provide faster particle formation rates which has a misleading effect on the impact of aerosols on climate.

Our results are especially meaningful for high-altitude new particle formation (e.g. in the upper troposphere and stratosphere). It has been previously reported the particle formation (Brock et al., 1995) and ion induced nucleation (Lee et al., 2003; English et al., 2011) as a source of new particles in high altitudes. In the upper troposphere and stratosphere general
20   circulation models coupled with aerosol dynamics models use aerosol evaporation as a source of [$H_2SO_{4(g)}$] (English et al., 2011). The concentration of $H_2SO_{4(g)}$ drastically affects new particle formation rates. The equilibrium constants for the dissociation and dehydration of H_2SO_4 reported in this study are needed to accurately model the sulphate aerosol particle evaporation and concentration of $H_2SO_{4(g)}$. They may also be important to evaluate particle formation schemes (homogeneous, ion-induced) for stratospheric conditions. These schemes are generally constrained based on tropospheric conditions (English
25   et al., 2011) but applied for stratosphere simulations._ Moreover, vapour–phase H_2SO_4 in the atmosphere appears to be ubiquitous, even in the absence of photochemistry (Mauldin et al. 2003; Wang et al., 2013); this may partly be due to evaporation of H_2SO_4 from aerosol particles.

In a changing climate it will become even more important to understand the thermodynamic properties of the sulphur aerosol particles involved in the development of polar stratospheric clouds and how sulphate aerosols influence the
30   stratospheric O_3 layer. Experiments simulating stratospheric conditions (*T≈200–265* K, *p≈10^{-1}–10^{-3}* atm, *RH≥1.0* % and *[H_2SO_4]≤10^8* molec.·cm^{-3}), are of great importance. Our results may also assist in explaining the atmospheric sulphur cycle of Venus. The Venusian clouds made up largely of sulphuric acid droplets cover an extended temperature range from 260 K

(upper clouds) to 310 K (middle clouds) and even higher (lower clouds). The scientific understanding of the upper tropospheric and stratospheric sulphate aerosol is of great importance for the global climate and requires further investigation.

5

10

15

20

25

Author Contributions

G.T. and J.D. designed and performed the experiments. G.T., J.D. and P.R. analysed the data. P.R. developed the model code. P.R. and G.T. performed the simulations. G.T., J. D., L. R., J. T., J. G. S., and A.K. collected the data and contributed to the analysis. G.T, P.R., J.D., and N.M.D assisted in drafting the manuscript. G.T., P. R., J. D., M. B., J. C., R. C. F., M. K., N. M. D., F. S. contributed to scientific interpretation and editing of manuscript. All authors contributed to the development of the CLOUD facility and analysis instruments, and commented on the manuscript.

Data availability

Requests for underlying material should be addressed to the corresponding author G.T (george.tsagkogeorgas@tropos.de).

References

Ayers, G. P., Gillett, R. W., and Gras, J. L.: On the vapour pressure of sulphuric acid, Geophys. Res. Lett. 7, 433–436, 1980.

Bollas, G. M., Chen, C.–C., and Barton, P. I.: Refined electrolyte–NRTL model: activity coefficient expressions for application to multi–electrolyte systems. AIChE J., 54, 1608–1624, 2008.

5 Brock, C. A., Hamill, P., Wilson, J. C., Jonsson, H. H., and Chan, K. R.: Particle Formation in the Upper Tropical Troposphere: A Source of Nuclei for the Stratospheric Aerosol, Science, Vol. 270, No. 5242, 1650-1653,1995.

Canagaratna, M. R., Jayne, J. T., Jimenez, J. L., Allan, J. D., Alfarra, M. R., Zhang, Q., Onasch, T. B., Drewnick, F., Coe, H., Middlebrook, A., Delia, A., Williams, L. R., Trimborn, A. M., Northway, M. J., DeCarlo, P. F., Kolb, C. E., Davidovits, P., and Worsnop, D. R.: Chemical and microphysical characterization of ambient aerosols with the Aerodyne aerosol mass 10 spectrometer, Mass Spectrom. Rev., 26, 185–222, 2007.

Capaldo, K., Corbett, J. J., Kasibhatla, P., Fischbeck, P. and Pandis, S. N.: Effects of ship emissions on sulphur cycling and radiative climate forcing over the ocean, Nature, 400, 743–746, 1999.

Charlson, R. J., Lovelock, J. E., Andreae, M. O., and Warren, S. G.: Oceanic phytoplankton, atmospheric sulphur, cloud albedo and climate, Nature, 326, 655–661, 1987.

15 Chen, C. C., Britt, H. I., Boston, J. F., Evans, L. B.: Local composition model for excess Gibbs energy of electrolyte systems. Part I: Single solvent, single completely dissociated electrolyte systems. AIChE J. 28, 588–596, 1982.

Clarke, A. D., Davis, D., Kapustin, V. N., Eisele, F., Chen, G., Paluch, I., Lenschow, D., Bandy, A. R., Thornton, D., Moore, K., Mauldin, L., Tanner, D., Litchy, M., Carroll, M. A., Collins, J., Albercook, G.: Particle nucleation in the Tropical boundary layer and its coupling to marine sulfur sources, Science, 282, 89–92, 1998a.

20 Clegg, S. L., and Brimblecombe, P.: Application of a Multicomponent Thermodynamic Model to Activities and Thermal Properties of 0–40 mol kg^{-1} Aqueous Sulfuric Acid from <200 to 328 K. J. Chem. Eng. Data, 40, 43–64, 1995.

Clegg, S. L., Brimblecombe, P., and Wexler, A.S.: Thermodynamic model of the system H^+–NH_4^+–Na^+–SO_4^{2-}–NO_3^-–Cl^-–H_2O at 298.5 K, J. Phys. Chem. A, 102, 2155–2171, 1998.

Curtius, J., Sierau, B., Arnold, F., Baumann, R., Schulte, P., and Schumann, U.: First direct sulfuric acid detection in the 25 exhaust plume of a jet aircraft in flight, Geophys. Res. Lett., **25**, 923–926, 1998.

Deshler, T.: A review of global stratospheric aerosol: Measurements, importance, life cycle, and local stratospheric aerosol, Atmos. Res., 90, 223–232, 2008.

Donahue, T. M., Hoffman, J. H., Hodges, R. R., and Watson, A. J.: Venus was wet: A Measurement of the Ratio of Deuterium to Hydrogen, Science, 216, 630–633, 1982.

30 Doyle, G. J.: Self–nucleation in the sulphuric acid–water system, J. Chem. Phys. 35, 795–799, 1961.

Drewnick, F., Schneider, J., Hings, S.S., Hock, N., Noone, K., Targino, A., Weimer, S., Borrmann, S.: Measurement of Ambient, Interstitial, and Residual Aerosol Particles on a Mountaintop Site in Central Sweden using an Aerosol Mass Spectrometer and a CVI, J. Atmos. Chem. 2006

Duplissy, J., Merikanto, J., Franchin, A., Tsagkogeorgas, G., Kangasluoma, J., Wimmer, D., Vuollekoski, H., Schobesberger, S., Ehrhart, S., Lehtipalo, K., Flagan, R., Brus, D., Donahue, N., Vehkamaki, H., Almeida, J., Amorim, A., Barmet, P., Bianchi, F., Breitenlechner, M., Dunne, E., Henschel, H., Junninen, H., Kirkby, J., Kurten, A., Kupc, A., Maattanen, A., Makhmutv, V., Napari, I., Nieminen, T., Praplan, A., Riccobono, F., Rondo, L., Steiner, G., Tome, A., Baltensperger, U., Carslaw, K., Dommen, L., Hansel, A., Petaja, T., Sipila, M., Stratmann, F., Vrtala, A., Wagner, P., Worsnop, D., Curtius, J., and Kulmala, M.: Effect of ions on sulfuric acid–water binary particle formation 2: Experimental data and comparison with QC–normalized classical nucleation theory, J. Geophys. Res. Atmos., 121, 1752–1775, 2016, doi:10.1002/2015JD023539.

English, J. M., Toon, O. B., Mills, M. J., and Yu, F.: Microphysical simulations of new particle formation in the upper troposphere and lower stratosphere Atmos. Chem. Phys., 11, 9303–9322, 2011

Fahey, D. W., Keim, E.R., Boering, K.A., Brock, C.A., Wilson, J.C., Jonsson, H.H., Anthony, S., Hanisco, T.F., Wennberg, P.O., Miake–Lye, R.C., Salawitch, R.J., Louisnard, N., Woodbridge, E.L., Gao, R.S., Donnelly, S.G., Wamsley, R.C., Del Negro, L.A., Solomon, S., Daube, B.C., Wofsy, S.C., Webster, C.R., May, R.D., Kelly, K.K., Loewenstein, M., Podolske, J.R., and Chan. K.R.: Emission measurements of the Concorde supersonic aircraft in the lower stratosphere, Science, 270, 70–74, 1995.

Fiedler, V., Dal Maso, M., Boy, M., Aufmhoff, H., Hoffmann, J., Schuck, T., Birmili, W., Hanke, M., Uecker, J., Arnold, F., and Kulmala, M.: The contribution of sulphuric acid to atmospheric particle formation and growth: a comparison between boundary layers in Northern and Central Europe, Atmos. Chem. Phys., 5, 1773–1785, 2005.

Fuchs, N. A. and Sutugin, A. G.: In Topics in Current Aerosol Research, Pergamon Press, 1971.

Galloway, J. N. and Rodhe, H.: Regional atmospheric budgets of S and N fluxes: how well can they be quantified? Proc. Roy. Soc. Edinburgh 97B, 61–80, 1991.

Giauque, W. F., Hornung, E. W., Kunzler, J. E., and Rubin, T. R.: The thermodynamic properties of aqueous sulphuric acid solutions from 15 to 300K, J. Am. Chem. Soc., 82, 62–70, 1960.

Gmitro, J. T. and Vermeulen, T.: Vapor–liquid equilibria for aqueous sulfuric acid, AIChEJ., 10, 740–746, 1964

Grädel, T. E. and Crutzen, P. J.: Chemie der Atmosphäre, Bedeutung für Klima und Umwelt (Spektrum, Heidelberg), 1994.

Hämeri, K., Väkevä, M., Hanson, H.–C., and Laaksonen, A.: Hygroscopic growth of ultrafine ammonium sulphate aerosol measured using an ultrafine tandem differential mobility analyzer, J. Geophys. Res., 105, 22 231–22 242, 2000.

Hanson, D. R. and Eisele, F.: Diffusion of H_2SO_4 in humidified nitrogen: Hydrated H_2SO_4, J. Phys. Chem., A, 104, 1715–1719, 2000.

Hashimoto, G. L. and Abe, Y.: Stabilization of Venus' climate by a chemical–albedo feedback, Earth Planet, Space, 52, 197–202, 2000.

21

Hoffman, J. H., Hodges, R. R., Donahue, T. M., and McElroy, M. B.: Composition of the Venus lower atmosphere from the Pioneer Venus mass spectrometer, J. Geophys. Res., 85, 7882–7890, 1980a.

Hommel, R., Timmreck, C. and Graf, H. F: The global middle–atmosphere aerosol model MAECHAM5–SAM2: comparison with satellite and in–situ observations, Geosci. Model Dev., 4, 809–834, 2011.

5   Hyvärinen, A.–P., Raatikainen, T., Laaksonen, A., Viisanen, Y., and Lihavainen, H.: Surface tensions and densities of H_2SO_4 + NH_3 + water solutions, Geophys. Res. Lett., 32, L16806, 2005.

Jacobson, M. Z.: Fundamentals of Atmospheric Modelling (2nd edition), Cambridge University Press, Cambridge, United Kingdom and New York, NY, USA, ISBN: 0 521 54865 9, 2005a.

Jayne, J. T., Pöschl, U., Chen, Y., Dai, D., Molina, L. T., Worsnop, D. R., Kolb, C. E., and Molina, M. J.: Pressure and 10   Temperature Dependence of the Gas–Phase Reaction of SO3with H2O and the Heterogeneous Reaction of SO3with H2O / H2SO4 Surfaces, J. Phys. Chem. A, 101, 10000–10011, 1997.

Jimemez, J.L., Jayne, J.T., Shi, Q., Kolb, C.E., Worsnop, D.R., Yourshaw, I., Seinfeld, J.H., Flagan, R.C., Zhang, X., Smith, K.A., Morris, J., Davidovits, P.: Ambient aerosol sampling with an aerosol mass spectrometer. J. Geophys. Res. – Atmospheres 108 (D7), 8425, 2003a.

15   Kiang, C. S., Stauffer, D.: Chemical nucleation theory for various humidities and pollutants, Faraday Symp. Chem. Soc., 7, 26–33, 1973.

Kiene, R. P.: Sulphur in the mix, Nature, 402, 363–365, 1999.

King, H. H., Hall, J. L., and Ware, G. C.: A study of the density, surface tension and adsorption in the water–ammonia system at 20°, J. Am. Chem. Soc., 52, 5128–5135, 1930.

20   Kirkby, J., Curtius, J., Almeida, J., Dunne, E., Duplissy, J., Ehrhart, S., Franchin, A., Gagné, S., Ickes, L., Kürten, A., Kupc, A., Metzger, A., Riccobono, F., Rondo, L., Schobesberger, S., Tsagkogeorgas, G., Wimmer, D., Amorim, A., Bianchi, F., Breitenlechner, M., David, A., Dommen, J., Downard, A., Ehn, M., Flagan, R., Haider, S., Hansel, A., Hauser, D., Jud, W., Junninen, H., Kreissl, F., Kvashin, A., Laaksonen, A., Lehtipalo, K., Lima, J., Lovejoy, E., Makhmutov, V., Mathot, S., Mikkilä, J., Minginette, P., Mogo, S., Nieminen, T., Onnela, A., Pereira, P., Petäjä, T., Schnitzhofer, R., Seinfeld, J., Sipilä, 25   M., Stozhkov, Y., Stratmann, F., Tomé, A., Vanhanen, J., Viisanen, Y., Aron Vrtala, A., Wagner, P., Walther, H., Weingartner, E., Wex, H., Winkler, P., Carslaw, K., Worsnop, D.,Baltensperger, U. and Kulmala, M.: Role of sulphuric acid, ammonia and galactic cosmic rays in atmospheric aerosol nucleation, Nature, 476, 429–433, 2011.

Kokkola, H., Hommel, R., Kazil, J., Niemeier, U., Partanen, A.–I., Feichter, J., and Timmreck, C.: Aerosol microphysics modules in the framework of the ECHAM5 climate model –intercomparison under stratospheric conditions, Geosci. Model 30   Dev., 2, 97–112, 2009.

Korhonen, P., Laaksonen, A., Batris, E., and Viisanen, Y.: Thermodynamics for highly concentrated water–ammonium sulfate solutions, J. Aerosol Sci., 29, 379–380, 1998b.

Kuang, C., McMurry, P. H., McCormick, A. V., and Eisele, F. L.: Dependence of nucleation rates on sulfuric acid vapor concentration in diverse atmospheric locations, J. Geophys. Res., 113, D10209, 2008.

Kulmala, M. and Laaksonen, A.: Binary nucleation of water–sulfuric acid system: Comparison of classical theories with different H_2SO_4 saturation vapor pressures, J. Chem. Phys., 93, 696–701, 1990.

Kulmala, M., Pirjola, L., and Mäkelä, J. M.: Stable sulphate clusters as a source of new atmospheric particles, Nature 404, 66–69, 2000.

5   Kürten, A., Rondo, L., Ehrhart, S., and Curtius, J.: Performance of a corona ion source for measurement of sulfuric acid by chemical ionization mass spectrometry, Atmos. Meas. Technol., 4, 437−443, doi: 10.5194/amt–4–437–2011, 2011.

Kürten, A., Rondo, L., Ehrhart, S. and Curtius, J.: Calibration of a Chemical Ionization Mass Spectrometer for the Measurement of Gaseous Sulfuric Acid, J. Phys. Chem. A, 116(24), 6375–6386, doi: 10.1021/jp212123n, 2012.

Laaksonen, A. and Kulmala, M.: Homogeneous heteromolecular nucleation of sulphuric acid and water vapours in
10 stratospheric conditions: A theoretical study of the effect of hydrate interaction, J. Aerosol Sci., 22, 779–787, 1991.

Lai, A. and Nazaroff, W. W.: Modelling indoor particle deposition from turbulent flow onto smooth surfaces, J. Aerosol Sci., 31, 463–476, 2000.

Lee, S.-H., Reeves, J. M., Wilson, J. C., Hunton, D. E., Viggiano, A. A., Miller, T. M., Ballentin, J. O., Lait L. R.: Particle formation by ion nucleation in the upper troposphere and lower stratosphere, Science 301, 1886–1889, 2003.

15 Lehtinen, K. E. J. and Kulmala, M.: A model for particle formation and growth in the atmosphere with molecular resolution in size, Atmos. Chem. Phys., 3, 251–257, 2003.

Margarella, A. M., Perrine, K. A., Lewis, T., Faubel, M., Winter, B., and Hemminger, J. C.: Dissociation of sulfuric acid in aqueous solution: Determination of the photoelectron spectral fingerprints of H_2SO_4, HSO_4^-, and SO_4^{2-} in water, J. Phys. Chem. C, 117, 8131–8137, 2013.

20 Marti, J. J., Jefferson, A., Ping Cai, X., Richert, C, McMurry, P. H., Eisele, F.: H_2SO_4 vapor pressure of sulfuric acid and ammonium sulfate solutions, J. Geophys. Res., 102, D3, 3725–3735, 1997.

Mauldin, R. L., III, Cantrell, C. A., Zondlo, M., Kosciuch, E., Eisele, F. L., Chen, G., Davis, D., Weber, R., Crawford, J., Blake, D., Bandy, A., and Thornton, D.: Highlights of OH, H_2SO_4, and methane sulfonic acid measurements made aboard the NASA P–3B during Transport and Chemical Evolution over the Pacific, J. Geophys. Res., 108(D20), 8796, 2003.

25 Mills, F. P., Esposito, L. W., and Yung, Y. L.: Atmospheric composition, chemistry, and clouds, In: Esposito, L. W., Stofan, E. R. and Cravens, T. E.(Eds.), Exploring Venus as a Terrestrial Planet, American Geophysical Union, Washington, DC, 73–100, 2007.

Moroz, V. I., Parfentev, N.A., and Sanko, N.F.: Spectrophotometric experiment on the Venera 11 and 12 descent modules. 2. Analysis of Venera 11 spectra by layer–addition method, Cosmis. Res. 17, 601–614, 1979.

30 Nickless, G.: Ed. "Inorganic Sulfur Chemistry", Elsevier, Amsterdam, 1968.

Noppel, M., H. Vehkamäki, and M. Kulmala, An improved model for hydrate formation in sulfuric–acid water nucleation, J. Chem. Phys, 116, 218–228, 2002.

Öm, G., Hansson U., and Rodhe, H.: Historical worldwide emissions of anthropogenic sulfur: 1860–1985, Department of Meteorology, Stockholm University, Report CM–91, 1996.

Petters, M. D. and Kreidenweis, S. M.: A single parameter representation of hygroscopic growth and cloud condensation nucleus activity, Atmos. Chem. Phys., 7, 1961–1971, 2007.

Pöschl, U., Canagaratna, M., Jayne, J. T., Molina, L. T., Worsnop, D. R., Kolb, C. E., and Molina, M. J.: Mass accommodation coefficient of H_2SO_4 vapor on aqueous sulfuric acid surfaces and gaseous diffusion coefficient of H_2SO_4 in N_2/H_2O, J. Phys. Chem. A 102:10082–10089, 1998.

Prinn, R. G.: Venus: Composition and Structure of the Visible Clouds, Science, 182, 1132–1135, 1973.

Que, H., Song, Y., and Chen, C.: Thermodynamic modeling of the sulfuric acid–water–sulfur trioxide system with the symmetric Electrolyte NRTL model. J. Chem. Eng. Data, 56, 963–977, 2011.

Rodhe, H.: Human impact on the atmospheric sulfur balance. Tellus, 51A–B, 110–122, 1999.

Roedel, W.: Measurements of sulfuric acid saturation vapor pressure: Implications for aerosol formation by heteromolecular nucleation, J. Aerosol Sci., 10, 375–386, 1979.

Roldin, P., Eriksson, A. C., Nordin, E. Z., Hermansson, E., Mogensen, D., Rusanen, A., Boy, M., Swietlicki, E., Svenningsson, B., Zelenyuk, A., and Pagels, J: Modelling non–equilibrium secondary organic aerosol formation and evaporation with the aerosol dynamics, gas– and particle–phase chemistry kinetic multilayer model ADCHAM, Atmos. Chem. Phys., 14, 7953–7993, 2014.

Roldin, P., Liao, L., Mogensen, D., Dal Maso, M., Rusanen, A., Kerminen, V.–M., Mentel, T. F., Wildt, J., Kleist, E., Kiendler–Scharr, A., Tillmann, R., Ehn, M., Kulmala, M., and Boy, M.: Modelling the contribution of biogenic volatile organic compounds to new particle formation in the Jülich plant atmosphere chamber, Atmos. Chem. Phys., 15, 10777–10798, 2015.

Simó, R. and Pedrós–Alió, C.: Role of vertical mixing in controlling the oceanic production of dimethyl sulphide, Nature, 402, 396–399, 1999.

Simpson, D., Fagerli, H., Hellsten, S., Knulst, J. C., and Westling O.: Comparison of modelled and monitored deposition fluxes of sulphur and nitrogen to ICP-forest sites in Europe, Biogeosciences, 3, 337–355, 2006.

Smith, S. J., Pitcher, H., and Wigley, T. M. L: Global and Regional Anthropogenic Sulfur Dioxide Emissions, Global Planet. Change, 29(1–2), 99–119, 2001.

Song, Y. and Chen, C.–C.: Symmetric Electrolyte Nonrandom Two–Liquid Activity Coefficient Model. Ind. Eng. Chem. Res., 48, 7788–7797, 2009.

Stauffer, D.:, Kinetic theory of two–component ("heteromolecular") nucleation and condensation, J. Aerosol Sci., 7, 319–333, 1976.

Sullivan, R. C., Petters, M. D., DeMott, P. J., Kreidenweis, S. M., Wex, H., Niedermeier, D., Hartmann, S., Clauss, T., Stratmann, F., Reitz, P., Schneider, J., and Sierau, B.: Irreversible loss of ice nucleation active sites in mineral dust particles caused by sulphuric acid condensation, Atmos. Chem. Phys., 10, 11471–11487, 2010.

Turco, R.P., Whitten, R.C., and Toon, O.B.: Stratospheric aerosols: Observation and theory, Rev. Geophys. Space Phys., 20, 233–279, 1982.

Vaida , V., Kjaergaard, H. G., Hintze, P. E., and Donaldson, D. J.: Photolysis of sulfuric acid vapor by visible solar radiation, Science, 299, 1566–1568, 2003.

Vehkamäki, H., Kulmala, M., Napari, I., Lehtinen, K. E. J., Timmreck, C., Noppel, M., and Laaksonen, A.: An improved parameterization for sulfuric acid–water nucleation rates for tropospheric and stratospheric conditions, J. Geophys. Res., 107(D22), 4622, 2002.

Volmer, M. and Weber, A.: Keimbildung in übersättigten Gebilden, Z. Phys. Chem., 119, 277, 1926.

Walrafen, G. E., Yang, W. H., Chu, Y. C., Hokmabadi, M. S.: Structures of Concentrated Sulfuric Acid Determined from Density, Conductivity, Viscosity, and Raman Spectroscopic Data, J. Solution Chem., 29, 905–936, 2000.

Wang, P., Anderko, A., Springer, R. D., and Young, R. D.: Modeling Phase Equilibria and Speciation in Mixed–Solvent Electrolyte Systems: II. Liquid–Liquid Equilibria and Properties of Associating Electrolyte Solutions. J. Mol. Liq., 125, 37–44, 2006.

Wang, S. C. and Flagan, R. C.: Scanning electrical mobility spectrometer, Aerosol Science and Technology 13.2, 230–240, 1990.

Wang, Z. B., Hu, M., Mogensen, D., Yue, D. L., Zheng, J., Zhang, R. Y., Liu, Y., Yuan, B., Li, X., Shao, M., Zhou, L., Wu, Z. J., Wiedensohler, A., and Boy, M.: The simulations of sulfuric acid concentration and new particle formation in an urban atmosphere in China, Atmos. Chem. Phys., 13, 11157–11167, 2013

Weber, R. J., McMurry, P. H., Mauldin, R. L., Tanner, D. J., Eisele, F. L., Clarke, A. D., and Kapustin, V. N.: New Particle Formation in the Remote Troposphere: A Comparison of Observations at Various Sites, Geophys. Res. Lett., 26, 307–310, 1999.

Wen, H. and Carignan, J.: Reviews on atmospheric selenium: Emissions, speciation and fate, Atmos. Env., 41, 7151–7165, 2007.

Wilson, J. C., Jonsson, H. H., Brock, C. A., Toohey, D. W., Avallone, L. M., Baumgardner, D., Dye, J. E., Poole, L. R., Woods, D. C., DeCoursey, R. J., Osborn, M., Pitts, M. C., Kelly, K. K., Chan, K. R., Ferry, G. V., Loewenstein, M., Podolske, J. R., Weaver, A.: In situ observations of aerosol and chlorine monoxide after the 1991 eruption of Mount Pinatubo: effect of reactions on sulfate aerosol, Science, 261, 1140–1143, 1993.

Yu, F. and Turco, R. P.: From molecular clusters to nanoparticles: Role of ambient ionization in tropospheric aerosol formation, J. Geophys. Res.–Atmos., 106, 4797–4814, 2001.

Zhang, X., Liang, M. C., Montmessin, F., Bertaux, J. L., Parkinson, C., and Yung, Y. L.: Photolysis of sulphuric acid as the source of sulphur oxides in the mesosphere of Venus, Nature, 3, 834–837, 2010.

Zuend, A., Marcolli, C., Luo, B. P., and Peter, T.: A thermodynamic model of mixed organic–inorganic aerosols to predict activity coefficients, Atmos. Chem. Phys., 8, 4559–4593, 2008.

Zuend, A., Marcolli C., Booth , A. M., Lienhard, D. M., Soonsin, V., Krieger, U. K., Topping, D. O., McFiggans G., Peter, T., and Seinfeld, J. H.: New and extended parameterization of the thermodynamic model AIOMFAC: calculation of activity

coefficients for organic–inorganic mixtures containing carboxyl, hydroxyl, carbonyl, ether, ester, alkenyl, alkyl, and aromatic functional groups, Atmos. Chem. Phys., 11, 9155–9206, 2011.

5

10

15

20

25

30

Table 1. Summary of the experimental conditions: temperature (T), relative humidity (RH), and gaseous sulphuric acid concentration ($[H_2SO_4]_{(g)}$), which is also given as saturation vapour pressure ($p_{sat,H2SO4}$) for each experiment.

Run No	CLOUD Run No	T (K)	RH (%)	$[H_2SO_4]_{(g)}$, peak (# cm^{-3})	$[H_2SO_4]_{(g)}$, background (# cm^{-3})	$p_{sat,H2SO4}$, peak (Pa)	$p_{sat,H2SO4}$, background (Pa)
1	914.01	288.8	10.1–0.5	$6.0 \cdot 10^7$	$1.2 \cdot 10^7$	$2.3 \cdot 10^{-7}$	$5.0 \cdot 10^{-8}$
2	914.06	288.8	3.5–0.5	$2.3 \cdot 10^8$	$1.0 \cdot 10^8$	$9.0 \cdot 10^{-7}$	$4.2 \cdot 10^{-7}$
3	919.02–04	268.0–293.0	1.4–0.3	$1.8 \cdot 10^9$	$2.0 \cdot 10^8$	$6.3 \cdot 10^{-6}$	$2.7 \cdot 10^{-7}$

5

10

15

20

ADCHAM model optimized – sulphur particle evaporation at low RH

Iteration procedure to calculate
particle phase composition & activity coefficients in equilibrium

Input parameters: RH, T, $K_{H_2SO_4}$, K_{SO_3}

Simulation procedure to calculate
particle number & phase chemistry in non-equilibrium

Input parameters: dN/d(logd$_P$), [H2SO4$_{(g)}$],
RH, T, p, chamber geometry

iteration loop continues until the error tolerance is fulfilled

Solve Ion Balance Equation

Calculated Molalities:
H_2SO_4, SO_3, H_2O,
HSO_4^-, SO_4^{2-}, NH_4^+, NH_3, H^+

Mole fractions
(anions, cations, molecules)

$$SO_{3(aq)} + H_2O \overset{K_{SO_3}}{\longleftrightarrow} H_2SO_{4(aq)}$$
$$\updownarrow K_{H_2SO_4}$$
$$HSO_{4(aq)}^- + H_3O^+$$
$$\updownarrow K_{HSO_4^-}$$
$$SO_{4(aq)}^{2-} + H_3O^+$$
$$NH_{3(aq)} + H^+ \overset{K_{NH_3}}{\longleftrightarrow} NH_4^+$$

Liquid phase: non ideal

Activities as a function of
water activity and particle size
$a_{H_2SO_4}$, a_{SO_3}, a_{H_2O},
$a_{HSO_4^-}$, $a_{SO_4^{2-}}$, $a_{N(III)}$, a_{H^+}

Aerosol dynamics

Dry deposition

Brownian coagulation

Saturation vapour pressures
(water, $H_2SO_{4(g)}$, $SO_{3(g)}$)

Updated particle size
and chemical composition
$dN/d\log dp$,
$[H_2SO_4]$, $[SO_3]$, $[H_2O]$,
$$\frac{N(-III)}{S(IV)}$$

Diffusivity
(H_2SO_4, SO_3)

Activity coefficients
$f_{H_2SO_4}$, f_{SO_3}, f_{H_2O}, $\gamma_{HSO_4^-}$, $\gamma_{SO_4^{2-}}$, $\gamma_{NH_4^+}$, γ_{H^+}

Gas-particle partitioning:
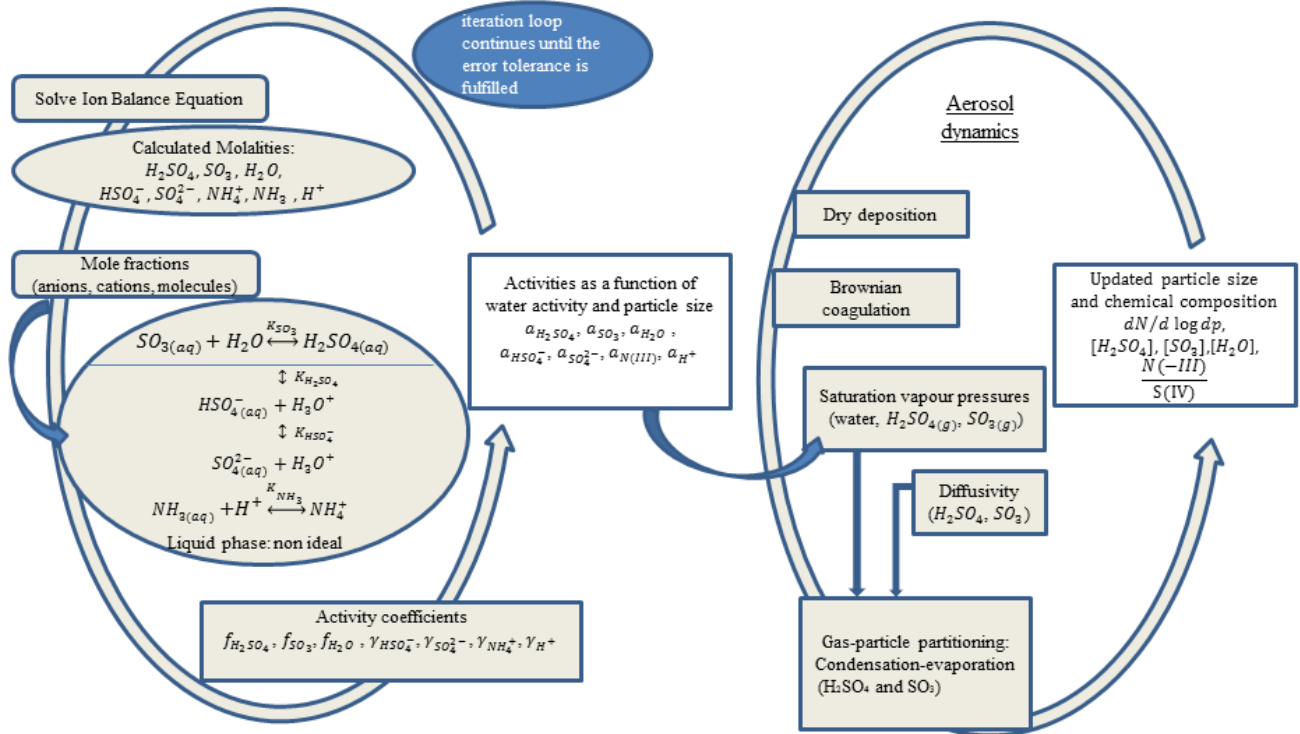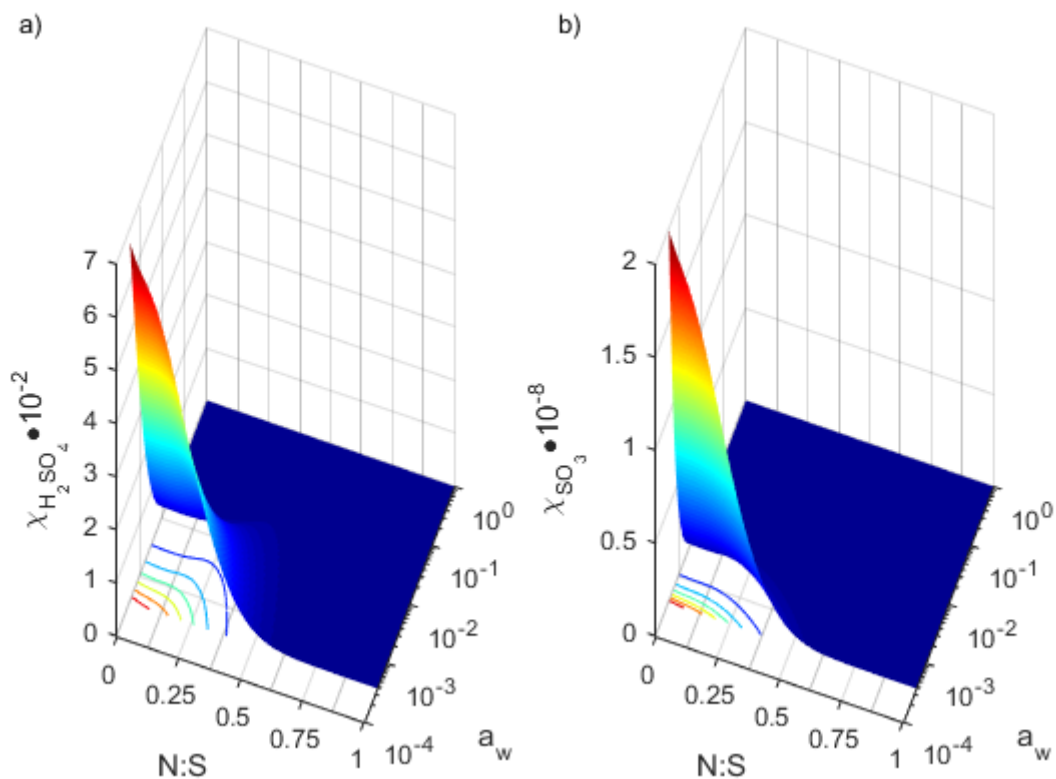Condensation-evaporation
(H2SO4 and SO3)

Figure 1. Schematic of the ADCHAM model optimized for the sulphur particle evaporation at low RH.

5

Figure 2. Modelled particle–phase mole fractions of (a) H₂SO₄(aq), $\chi_{H_2SO_4}$, and (b) SO₃(aq), χ_{SO_3}, as a function of the water activity (a_w) and the *N:S* for Case 2a which represents the combination of H₂SO₄, H₂O and SO₃ evaporating species with H₂SO₄ being the dominating evaporating S(VI) species. The colour coded contours on x–y axes represent constant particle–phase mole fractions for a) $\chi_{H_2SO_4}=1–6\cdot10^{-2}$ and b) $\chi_{SO_3}=0.3–1.8\cdot10^{-8}$. The equilibrium coefficients are $K_{H_2SO_4}=2.40\cdot10^9$ mol·kg⁻¹, and $^xK_{SO_3}=1.43\cdot10^{10}$ at T=288.8 K.
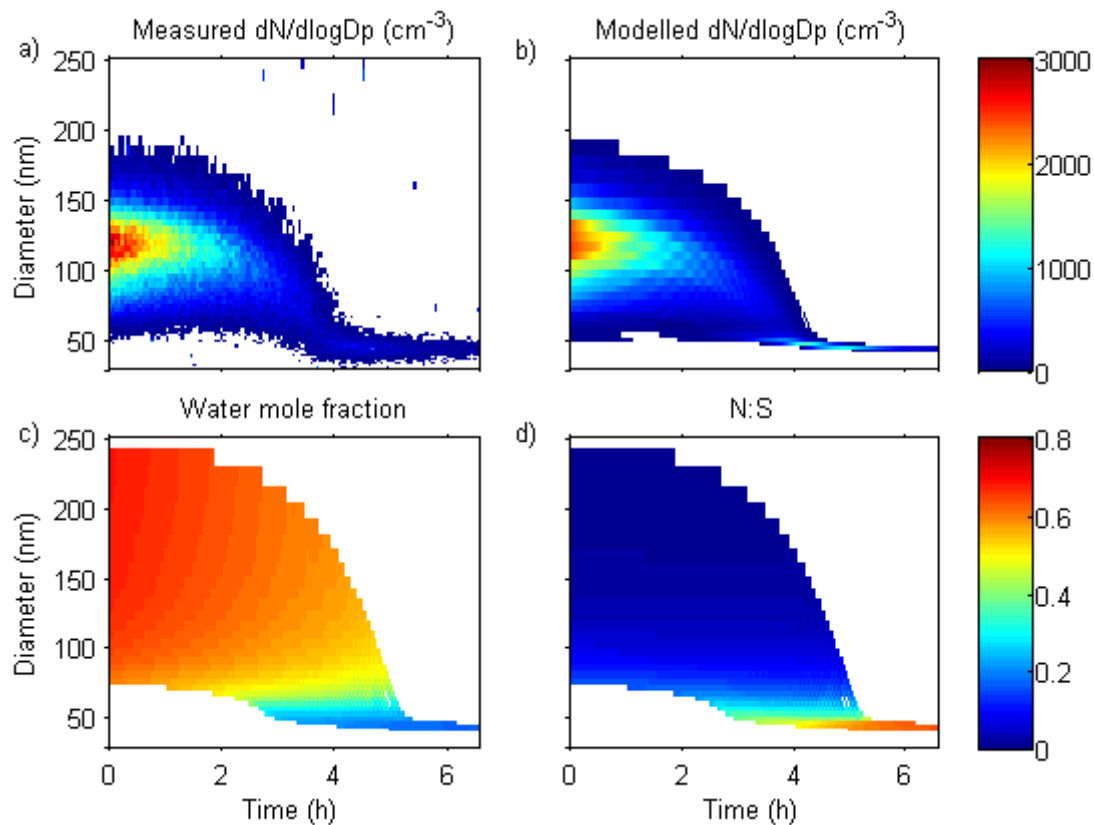
Figure 3. Particle shrinkage at low RH. Measured (a) and modelled (b) particle number size distribution evolution during experiment 2 performed at $T=288.8$ K for Case 2a with H_2SO_4 being the dominating evaporating S(VI) species, $K_{H_2SO_4}=2.40 \cdot 10^9$ mol·kg^{-1} and $^x K_{SO_3}=1.43 \cdot 10^{10}$. Figures (c) and (d) show the modelled particle water mole fraction, χ_{H_2O} and N:S, respectively.
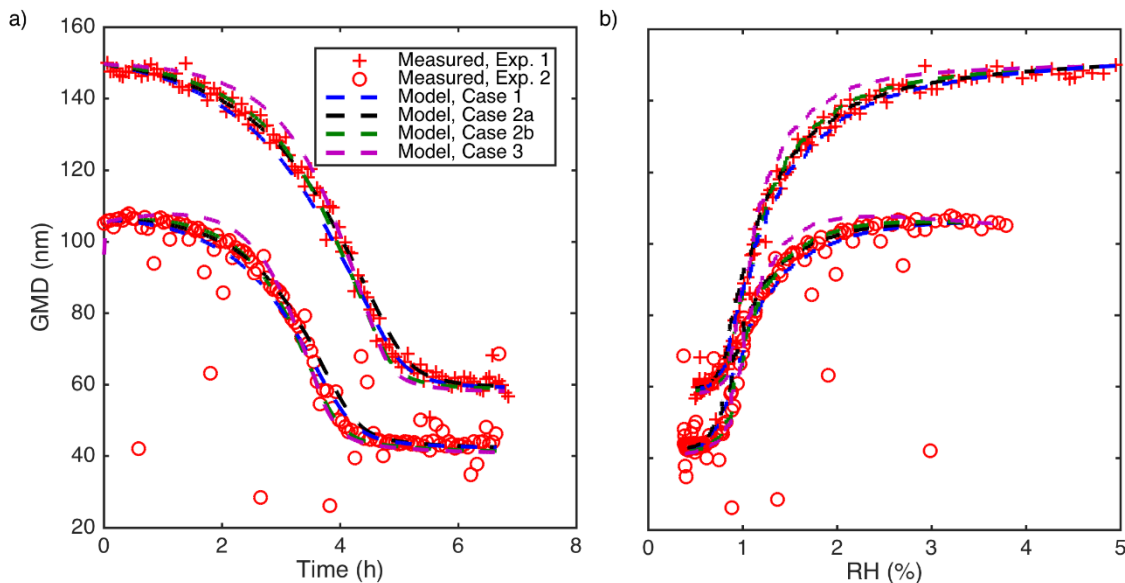
5

Figure 4. Measured and modelled GMD evolution as a function of (a) time and (b) RH for experiments 1 and 2 performed at *T=288.8* K. The modelled particles are composed of S(VI), H₂O and NH₃ as a particle phase contaminant. The simulations correspond to Case 1 with H₂SO₄ being the only evaporating S(VI) species, $K_{H_2SO_4}$=*2.00·10⁹* mol·kg⁻¹, Case 2a with H₂SO₄ being the dominating evaporating S(VI) species, $K_{H_2SO_4}$=*2.40·10⁹* mol·kg⁻¹ and $^xK_{SO_3}$ =*1.43·10¹⁰*, Case 2b with SO₃ being the dominating evaporating S(VI) species, $K_{H_2SO_4}$ =*4.00·10⁹* mol·kg⁻¹ and $^x K_{SO_3}$ =*1.54·10⁹* and Case 3 with SO₃ being the only evaporating S(VI) species, $K_{H_2SO_4}$=*1.00·10¹¹* mol·kg⁻¹ and $^xK_{SO_3}$=*3.33·10⁷* (see Supplement, Table S1, simulations 1–4 and 13–16). The pure liquid saturation vapour pressures of H₂SO₄ and SO₃ are calculated with Eq. (11), N–K–L parameterisation, (Kulmala and Laaksonen (1990) and Noppel et al., 2002) and Eq. (12) (Nickless, 1968), respectively.
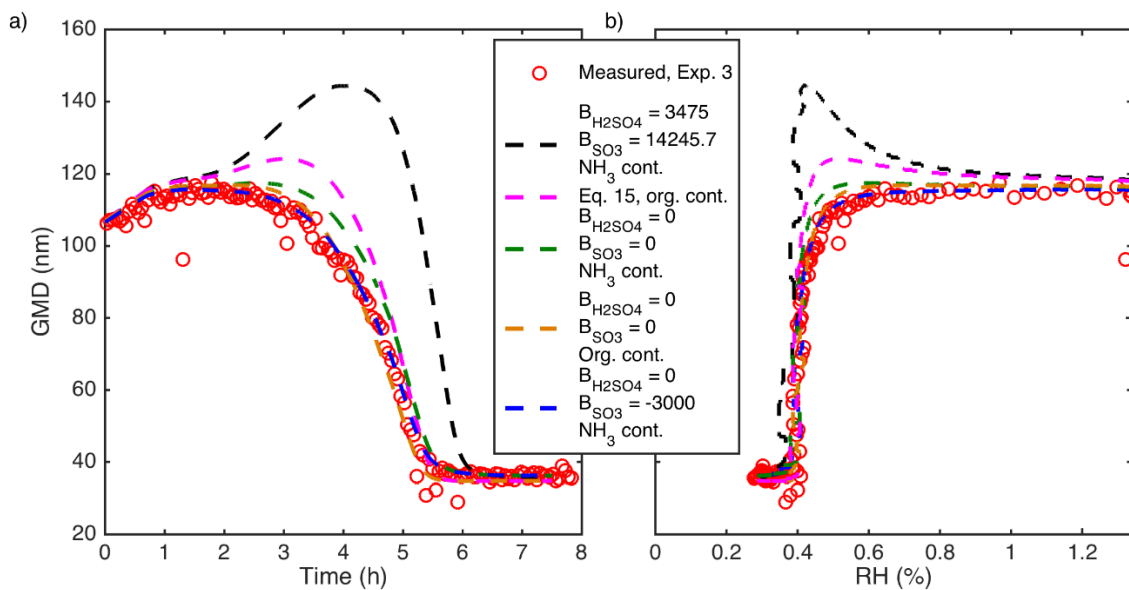
Figure 5. Measured and modelled GMD evolution as a function of (a) time and (b) RH for experiment 3 performed at a temperature range from 268 K to 293 K. The modelled particles are composed of S(VI), H₂O and either NH3 or non–volatile, non–water–soluble organics as a particle phase contaminant. The simulations correspond to Case 1 (the H₂SO₄ activity is calculated with use of Eq. (15) and the tabulated H₂SO₄ chemical potentials from Giauque et al. (1960), see Supplement, Table S1, simulation 28) and Case 2a, $K_{H_2SO_4}=2.40\cdot10^9$ mol·kg⁻¹ and $^xK_{SO_3}=1.43\cdot10^{10}$ at $T=288.8$ K, (see Supplement, Table S1, simulations 29, 33, 34 and 36). The pure liquid saturation vapour pressures of H₂SO₄ and SO₃ are calculated with Eq. (11) (Kulmala and Laaksonen (1990) and Noppel et al., 2002) and Eq. (12) (Nickless, 1968), respectively.

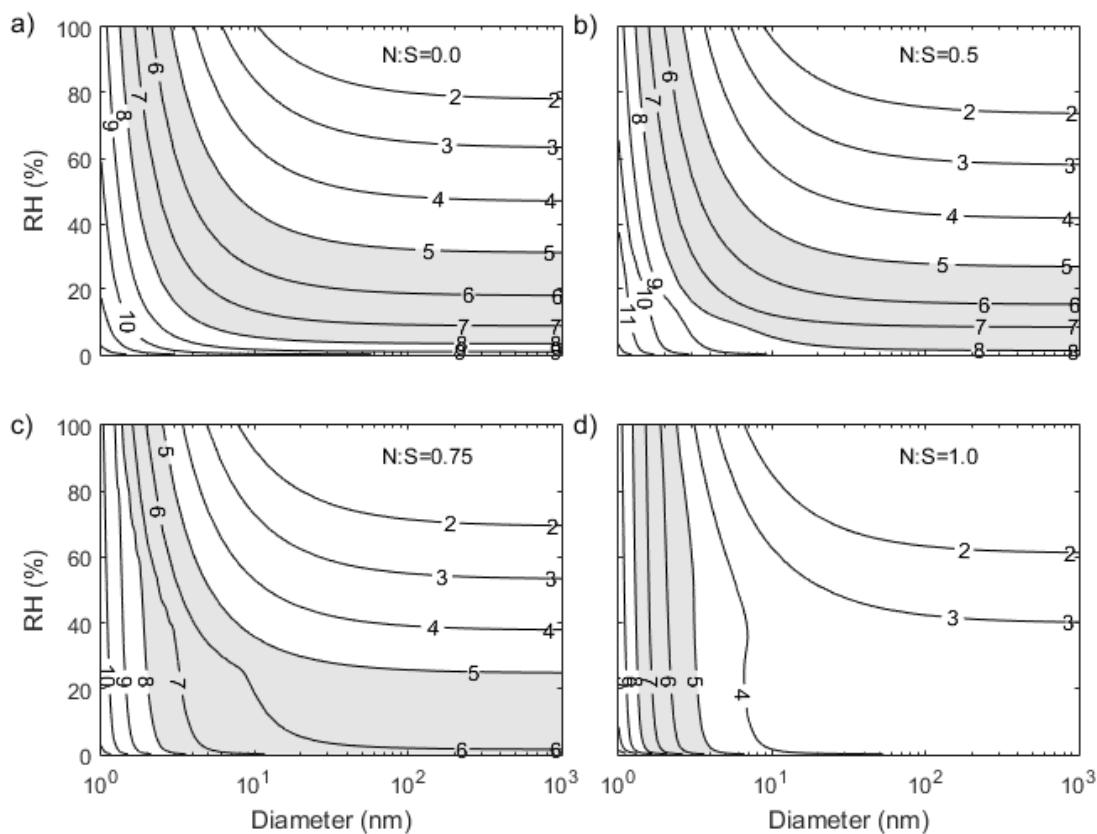**Figure 6.** Modelled effective H₂SO₄ saturation concentration, $C^*_{H_2SO_4,S}$, (molecules·cm⁻³), expressed in $log_{10}(C^*_{H_2SO_4,S})$, at T=288.8 K, RH 0–100 % and particle diameters in the range from 1 to 10^3 nm. The contours represent H₂SO₄ gas–phase concentrations, e.g. $log_{10}(C^*_{H_2SO_4,S})$, =7 corresponds to $C^*_{H_2SO_4,S}$=10^7 molecules·cm⁻³. The grey shading indicates the atmospheric range of H₂SO₄ ($10^{5–}$ 10^8 cm⁻³). The results correspond to particles composed (a) only of S(VI) and H₂O (N:S=0), (b) with N:S=0.5, (c) with N:S=0.75 and (d) with N:S=1. The equilibrium constants are $K_{H_2SO_4}$=2.40·10^9 mol·kg⁻¹ and $^xK_{SO_3}$=1.43·10^{10}. The pure liquid saturation vapour pressures of H₂SO₄ and SO₃ are calculated with Eq. (11) and (12).